



NTNU – Trondheim
Norwegian University of
Science and Technology

Numerical Analysis of Condensation and Frost in Rotary Heat Exchangers

Erlend Tunå

Master of Energy and Environmental Engineering

Submission date: June 2014

Supervisor: Hans Martin Mathisen, EPT

Norwegian University of Science and Technology
Department of Energy and Process Engineering

EPT-M-2014-123

MASTER THESIS

for

Student Erlend Tunå

Spring 2014

Numerical analysis of condensation and frosting in rotary heat exchangers

*Numerisk analyse av kondensasjon og frost i roterende varmegjenvinnere***Background and objective**

In a rotary heat exchanger during cold conditions water vapour might condense on the exhaust side and be transferred to fresh air side. During conditions with dry indoor air this is an advantage, but at high indoor moisture production the relative humidity of the indoor air may become too high. At low outdoor temperatures the exchanger might be blocked due to frosting. Different mechanisms also lead smell to be transferred from the exhaust to fresh air.

The aim of the thesis is to present flow conditions and temperature variations in a rotating heat exchanger under conditions that do not give rise to condensation and consider when condensation may occur. Moreover, it is desirable that the effect of absorption is evaluated and demonstrated, and that condensation and frost are included in the model.

The following tasks are to be considered:

1. Literature survey on use of relevant numerical methods/tools for heat exchangers
2. Decide what type of tool to use
3. Describe the exchanger to be simulated and its boundary conditions
4. Establish models and performs simulations
5. Evaluate results against effectiveness and conditions for condensation described in the project thesis.

-- ” --

Within 14 days of receiving the written text on the master thesis, the candidate shall submit a research plan for his project to the department.

When the thesis is evaluated, emphasis is put on processing of the results, and that they are presented in tabular and/or graphic form in a clear manner, and that they are analyzed carefully.

The thesis should be formulated as a research report with summary both in English and Norwegian, conclusion, literature references, table of contents etc. During the preparation of the text, the candidate should make an effort to produce a well-structured and easily readable report. In order to ease the evaluation of the thesis, it is important that the cross-references are correct. In the making of the report, strong emphasis should be placed on both a thorough discussion of the results and an orderly presentation.

The candidate is requested to initiate and keep close contact with his/her academic supervisor(s) throughout the working period. The candidate must follow the rules and regulations of NTNU as well as passive directions given by the Department of Energy and Process Engineering.

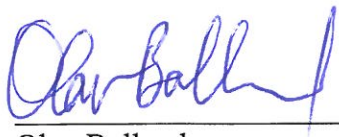
Risk assessment of the candidate's work shall be carried out according to the department's procedures. The risk assessment must be documented and included as part of the final report. Events related to the candidate's work adversely affecting the health, safety or security, must be documented and included as part of the final report. If the documentation on risk assessment represents a large number of pages, the full version is to be submitted electronically to the supervisor and an excerpt is included in the report.

Pursuant to "Regulations concerning the supplementary provisions to the technology study program/Master of Science" at NTNU §20, the Department reserves the permission to utilize all the results and data for teaching and research purposes as well as in future publications.

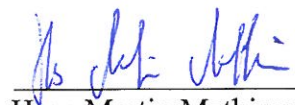
The final report is to be submitted digitally in DAIM. An executive summary of the thesis including title, student's name, supervisor's name, year, department name, and NTNU's logo and name, shall be submitted to the department as a separate pdf file. Based on an agreement with the supervisor, the final report and other material and documents may be given to the supervisor in digital format.

- Work to be done in lab (Water power lab, Fluids engineering lab, Thermal engineering lab)
 Field work

Department of Energy and Process Engineering, 14. January 2014



Olav Bolland
Department Head



Hans Martin Mathisen
Academic Supervisor

Research Advisor:
Reidar Kristoffersen

Summary

In this thesis, a three-dimensional mathematical model is developed and implemented using *COMSOL Multiphysics* - a platform for physics-based modeling and simulation. The numerical model solves a conjugated heat transfer problem for the air stream and heat exchange media with only wheel data and inlet flow properties needed as input. The model was validated using previously established effectiveness correlations for a comparable regenerative heat exchanger but needs further validation.

Proper scaling analysis was performed to establish the simultaneously developing Nusselt numbers in the entrance region from incomplete tabular data sources, and a new local peripheral Nusselt number function was defined from the flow geometry to take into account the variable local heat flux around the periphery.

Results indicate that the local properties at any cross-section may differ significantly from the bulk properties, suggesting that condensation may be present locally in pockets of near-stagnant regions for a considerable length of the wheel.

Sammendrag

I denne tesen har en tre-dimensjonal matematisk modell blitt utviklet og implementert ved hjelp av *COMSOL Multiphysics* – som er en platform for fysikk-basert modellering og simulasjon. Den numeriske modellen er klassifisert som et konjugerende varmetransport problem for luftstrømningen og varmeoverføringsmediet og er kun avhengig av data for hjulet og luft-innstrømningene. Modellen er validert mot tidligere etablerte effektivitets korrelasjoner for en tilsvarende varmeveksler men trenger oppfølgingsanalyser.

Skaleringsanalyse ble utført for å etablere de samtidige utviklende Nusselt numrene i starten av kanalen fra inkomplette tabulære data kilder, og en ny lokal Nusselt nummer funksjon ble definert fra strømningsgeometrien for å ta hensyn til den variende lokale varmefluksen rundt periferien av et tverrsnitt.

Resultatene indikerer at lokale forhold ved et tverrsnitt kan skille seg betraktelig fra gjennomsnittet og således kan kondensasjon eksistere i lommer med lav lufthastighet for en vesentlig del av hjulets lengde.

Table of Contents

Summary	i
Table of Contents	iii
Nomenclature	v
1 Introduction	1
2 The Components of a Computational Fluid Dynamics Simulation System	5
2.1 Defining the Mathematical Model / 5	
2.2 Defining the Discretization Process / 6	
2.3 Performing the Analysis Phase / 7	
2.4 Defining the Resolution Phase / 7	
2.5 Features of COMSOL Multiphysics / 9	
3 Mathematical Model	11
3.1 Geometry / 11	
3.2 Assumptions / 12	
3.3 Conservation of Mass and Force Balances (Momentum Equations) / 14	
3.4 First Law of Thermodynamics / 18	
3.4.1 Conjugated Heat Transfer Problem / 18	
3.4.2 Thermal Boundary Conditions / 20	
3.5 Mass Conservation of Constituents in the Air Stream / 22	
3.6 Conjugated Heat and Mass Transfer Problem / 24	
4 Numerical Model	29
4.1 Defining the Global Parameters / 29	

4.2	Defining the Sine Geometry / 29	
4.3	Velocity Problem / 32	
4.4	Conjugated Heat Transfer Problem / 34	
4.4.1	Averaged Peripheral Nusselt Number / 36	
4.4.2	Local Peripheral Nusselt Number / 42	
4.4.3	Defining the Bulk Temperature / 47	
4.4.4	Imposing the Thermal Boundary Conditions / 50	
4.5	Mass Conservation of Constituents in the Air Stream / 52	
4.6	Space Discretization (Grid Generation) / 53	
4.7	Pseudo Steady-State and Livelink for Matlab / 57	
5	Results and Discussion	61
5.1	Mesh Refinement Study / 61	
5.2	Validation of Formulation / 63	
5.3	Test Case / 66	
6	Conclusions and Future Areas of Study	71
	References	73
A	Moist Air Theory	
B	Numerical Algorithm	
C	Running a Job on the Kongull Linux Cluster	

Nomenclature

English Symbols

a	<i>half height of the sine duct [m]</i>
A_{fr}	<i>wheel frontal area [m²]</i>
A_s	<i>heat transfer surface area in one sector [m²]</i>
A_c	<i>cross-sectional flow area [m²]</i>
A	<i>total heat transfer surface area [m²]</i>
b	<i>half width of the sine duct [m]</i>
c	<i>molar concentration [mol / m³]</i>
Cr_0^*	<i>overall matrix heat capacity</i>
Cr	<i>matrix heat capacity rate [W / K]</i>
C^*	<i>ratio of minimum to maximum air stream heat capacity rate</i>
C_p	<i>specific heat at constant pressure [J/kg · K]</i>
d	<i>distance from centroid of maximum velocity [m] or coefficient</i>
d_s	<i>shell thickness [m]</i>
D_h	<i>hydraulic diameter [m]</i>
D	<i>mass diffusivity [m² / s]</i>
e	<i>coefficient</i>
f	<i>friction factor, local peripheral Nusselt number function or source term</i>
\mathbf{F}	<i>volume force vector [N/m³]</i>

h	<i>convective heat transfer coefficient</i> $[W/m^2 \cdot K]$
h_m	<i>convective mass transfer coefficient</i> $[m/s]$
H	<i>enthalpy</i> $[kJ/kg \cdot K]$
\mathbf{j}	<i>diffusion flux vector</i>
k	<i>thermal conductivity</i> $[W/m^2 \cdot K]$
L	<i>length</i> $[m]$
\dot{m}	<i>mass flow rate</i> $[kg/s]$
M	<i>matrix mass</i> $[kg]$ <i>or molecular weight</i> $[kg/kmol]$
n	<i>numerical coefficient</i>
N	<i>angular speed</i> $[rev/s]$
Nu	<i>Nusselt number</i>
NTU_0	<i>overall number of heat transfer units</i>
p	<i>pressure</i> $[Pa]$ <i>or period</i> $[s]$
P	<i>perimeter</i> $[m]$
Pr	<i>Prandtl number</i>
Pe	<i>Peclet number</i>
Q_{oop}	<i>out-of-plane heat transfer</i> $[W/m^2]$
q'	<i>perimeter line integral of heat flux</i> $[W/m]$
q''	<i>heat flux</i> $[W/m^2]$
\mathbf{q}	<i>conduction heat flux vector</i> $[W/m^2]$
Re	<i>Reynolds number</i>

s distance along perimeter [m]

T absolute temperature [K]

t time [s]

\mathbf{u} velocity vector [m/s]

u, v, w velocity components [m/s]

w mass fraction [kg / kg]

x, y, z spatial coordinates [m]

z^* dimensionless axial coordinate

Greek Letters

ρ density [kg/m³]

μ dynamic viscosity [N · s/m²]

Γ boundary around the periphery

φ relative humidity

α area correcting factor or thermal diffusivity

α^* ratio of sine height to sine length

β local area goodness factor function or matrix packing density [m² / m³]

σ wheel porosity [m² / m²]

ε effectiveness

ξ dummy variable

δ_T *thermal boundary layer thickness [m]*

δ *velocity boundary layer thickness [m]*

γ *local area goodness factor*

Subscripts

ave *average in channel*

b *bulk*

e *exhaust*

face *face of wheel*

fd *fully developed*

i *constituent*

m *mixture or mean*

min *minimum*

max *maximum*

p *perimeter*

s *supply*

0 *reference or initial value*

CHAPTER 1

INTRODUCTION

In a rotary regenerator (or regenerative heat exchanger) heat and moisture is cyclically transferred from one of the air streams to the matrix and then to the other air stream as shown in Figure 1.1. If the regenerator is designed to only transfer sensible heat (temperature) it is termed a heat wheel (and sometimes rotating heat exchanger) and the heat transfer is only driven by the temperature difference between the two air streams. When the wheel in addition is designed to transfer latent heat (moisture) through a desiccant coated layer on the surface of the rotor material by exploiting water vapor concentration differences in the air streams, it is called an energy wheel (and sometimes a enthalpy wheel or desiccant-coated heat wheel). Typical operating conditions for the two types of wheels is presented in Figure 1.2 on a Mollier chart. We observe that under winter conditions moisture transfer occurs in the cold part of the heat wheel due to condensation, but that no moisture transfer will take place during the summer. As the energy wheel transfer moisture through sorption during both winter and summer conditions, the outlet conditions of the airflows end up on an intermediate line between the two inlet conditions (Tunaa, 2013).

The majority of the total heat exchange media used in energy wheels for air-conditioning today is generally aluminum foil substrate with a surface coating of a desiccant material consisting of a dry film of silica gel or molecular sieve ((Fischer Jr, 1988; Jeong and Mumma, 2005), but we may also find oxidized surfaces or a separate coating of aluminum oxide. The desiccant material account for about 20 percent of the energy wheel mass, and as such the bulk of sensible heat transfer is accomplished through the aluminum portion of the wheel as for heat wheels without a desiccant coating. Simonson, Besant, and Wilson (1997) contributes the aluminum wheels high thermal conductivity and thermal capacitance for its popularity in air-conditioning where high sensible and latent heat transfer is usually desired, while Fischer Jr. (1988) also credit it for its high strength and durability and also the advantage that aluminum in some cases is capable of being washed with water or steam without harming the desiccant coating (Tunaa, 2013).

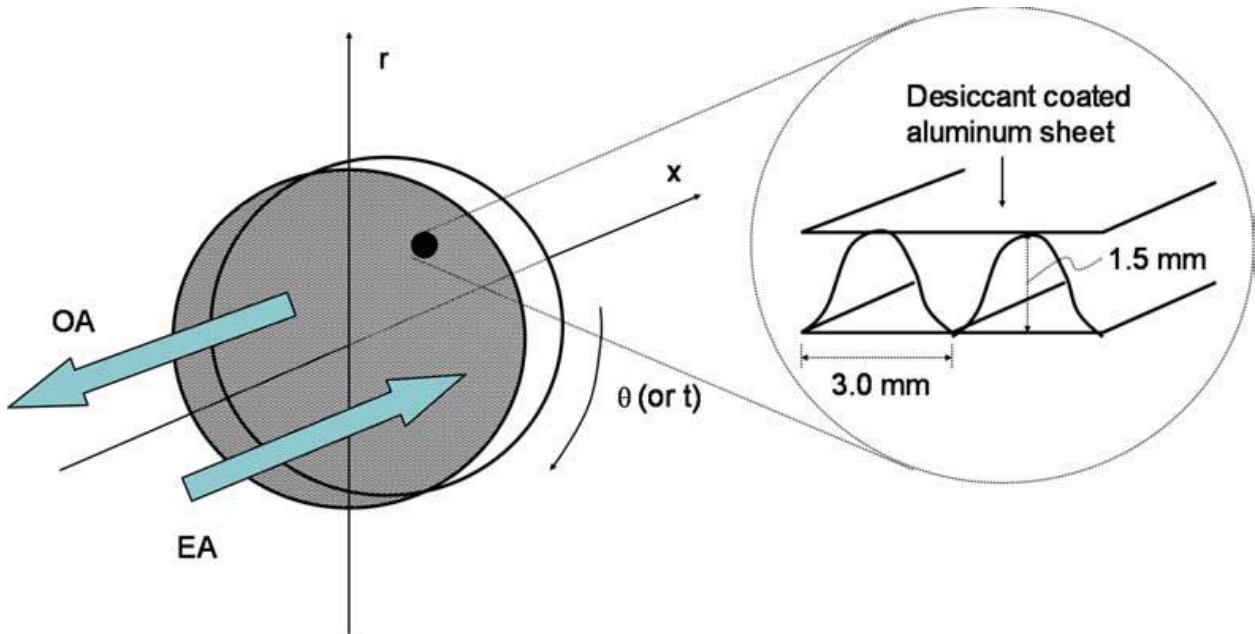


Figure 1.1 Conceptual drawing of the wheel geometry (From Jeong and Mumma, 2005)

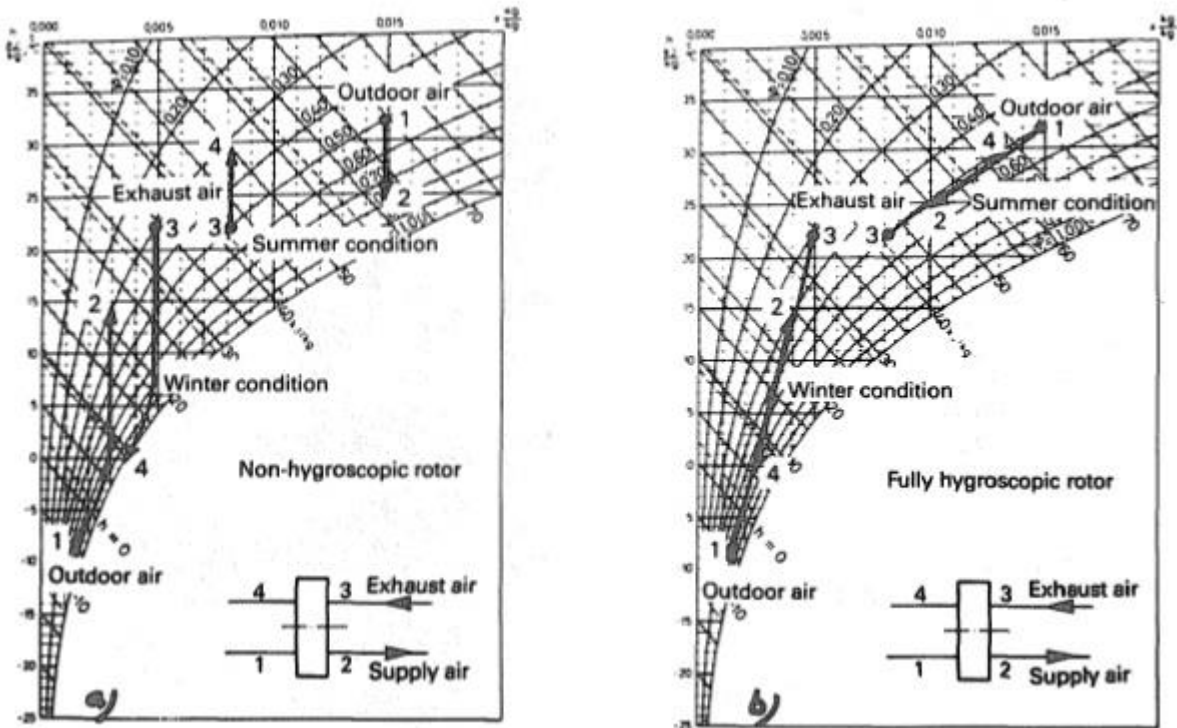


Figure 1.2 Illustration of winter and summer operations of (a) heat wheel, and (b) energy wheel (From Holmberg, 1989)

The sensible and latent heat exchange media used in the wheels are generally in the form of a matrix that provides small, uninterrupted flow channels through which an air stream can flow (Fischer Jr, 1988). A common matrix arrangement for air-conditioning purposes is a type of honeycomb matrix, where alternating layers of a corrugated sheet material and a flat sheet material is formed to produce e.g. the sinusoidal curve as shown in Fig. 1.1, that extends axially along the depth of the wheel. The effectiveness of the wheel matrix is strongly correlated to the heat/mass transfer surface area to volume ratios. The small flow passages provides a large surface area, in the order of $1000-5000 \text{ m}^2/\text{m}^3$, so that it is possible to transfer a lot of energy with very compact wheels, making high heat and moisture transfer effectiveness a characteristic of heat/energy wheels (Simonson, 2007; Tunaa, 2013).

One problem associated with the use of rotary regenerators is that of condensation and frosting under winter conditions. As the warm and humid exhaust air passes through the heat exchange media, it can be cooled to the dew point temperature and a thin film of condensate will then start to form on the surface. Excessive or uncontrolled condensation may severely degrade the desiccant coating used in energy wheels if the desiccant is saturated and water begins to run off and, if the temperature is below freezing, frost may begin to accumulate within the exchanger, potentially restricting air flow and reduce the effectiveness or damage equipment (Simonson et al., 1997). Rotary regenerators may however operate with frost or condensation occurring on the rotor surfaces under controlled conditions, since the condensate is evaporated and frost sublimated on the supply air side (Holmberg, 1989). In comparison with static heat recovery units, such as plate heat or membrane exchangers, where the frost layer will grow in thickness as more condensate precipitates out onto the cold surface, the moisture transfer in heat/energy wheels will effectively lower the limiting temperature for which frost accumulation will occur (Holmberg, 1989; Tunaa, 2013).

This problem of condensation and frost in heat and energy wheels has been investigated by several researchers, with Holmberg (1989) predicting the condensation/frost limits for both heat and energy wheels, and Simonson et al. (1997) and Bilodeau et al. (1999) analyzing the case of energy wheels. The former produces some interesting charts where heat/energy wheels can be directly compared, while the latter two is more detailed in that they in addition to analyzing the location of the condensation/frost zones also simulates the frost-build up over time. The investigation by Bilodeau et al. (1999), employing a three-dimensional formulation, as opposed to the one-dimensional channel considered in the other investigations, is especially interesting as it also analyzes the effect of time on the frosting limit.

The common denominator among all of these investigations is however that they all are written in imperative programming languages like *Fortran*, and that information are at best scarce regarding the modeling parameters (with the exception of Simonson (1998) in which all

the wheel parameters are given and numerical code provided) and various diffusion and transfer coefficients used. As such these formulations and their numerical implementation remains for all purposes inaccessible to the designer with results that are hard to reproduce, let alone analyzing and customizing for design purposes.

With that in mind the objective of this thesis is to develop a three-dimensional mathematical model describing the flow geometry and heat transfer in a single sine duct from first principles and translate the resulting formulation into a numerical model using the computational package *COMSOL Multiphysics*. The numerical model will be constructed with ease of use in mind so that the designer will be able to control the entire model using just the modeling parameters which includes all of the geometry parameters and the operating conditions. This means that the designer is free to make changes to any of the modeling parameters with all the components of the model, including the geometry and physics, automatically adjusting to the current input parameters (the only exception to this is the heat transfer coefficient which will vary based on the thermal boundary condition used).

As mass transfer is neglected the model will represent a regenerative heat exchanger or heat wheel without sorption or condensation/frosting (mass transfer), but still as the concentration field will be solved for, we will be able to retrieve information on whether or not there is a risk for condensation on any local cold spots. The decision not to include mass transfer is that it would require additional considerations that are better explored when having successfully completed this first step as the same physics are used. The present model is however constructed with this future objective in mind, and will as such provide a useful comparison for a model using the same template but having successfully incorporated the additional physics needed to represent a heat/energy wheel with or without condensation.

Due to not being able to complete the numerical model in a timely fashion (a result of licensing issues and the sheer complexity of the complete numerical model) the resulting model has not been excessively analyzed. The problem has been one of trading time working with the numerical model on the desktop (which for the most part has been necessary in compiling this paper) and simulating as the number of licenses only on rare occasions has allowed for both. Moreover as the memory required has proven too be far too extensive for laptops (at least for single-core ones) it has been necessary to outsource the computations, and given the stretches of time needed when simulating, the process at times obviously has been less than ideal. As a result the model has not gone through a mesh refinement study nor has it been the subject of extensive validation procedures. Not having enough licenses to orchestrate parallel computations in order to compile a data set of different modeling parameters, only the results of one test case has been analyzed.

CHAPTER 2

THE COMPONENTS OF A COMPUTATIONAL FLUID DYNAMICS SIMULATION SYSTEM

The objective of this thesis is to establish a model that encompasses the physics at play in a regenerative heat exchanger and to simulate how that model, woven together by a system of equations representing the physics, responds to changing operating conditions. For that we need a platform for physics-based modeling and simulation that allows us to complete a series of steps as shown in the chart below (Figure 2.1). In what follows we will take a look at each of these in turn and note the differences between an imperative programming language like *Fortran* (derived from Formula Translating System) and computational packages like *COMSOL Multiphysics*. In the former all the sequences of commands that the computer is to perform has to be defined by the user, allowing for custom designed numerical techniques and processing. In the latter a set of predefined interfaces, couplings and operations contained within a *Model Tree* that spans all the steps are available and are presented on a graphical interface that allows for ongoing visual feedback. This is the approach taken in this thesis.

2.1 Defining the Mathematical Model

The first step in setting up the simulation is to define the physics that is to be simulated. In the next chapter the theoretical background for the mathematical model is presented along with any modeling assumptions made. In the case of a graphical user interface processor such as *COMSOL Desktop* the mathematical model can then be directly formulated using the appropriate physics with initial and boundary conditions, parameters, variables, couplings and so forth on a geometry built using a computer-aided design (CAD) software. This is the objective of the chapter describing the numerical implementation of the mathematical model.

If *Fortran* is used we still have to define the parameters, variables, couplings and so forth, but there is no need to set up the governing equations as only the discretized space domain and model equations is used in the computational sequences. At the base level the graphical user interface reduces to computing language, but clearly there is an advantage in working graphically as it presumably is less time-consuming and the ongoing feedback will make the user less prone to making errors.

In any regard it should be emphasized that within the world of continua, as currently applied to describe the behavior of fluids and solids, there is always an unavoidable level of

empiricism in the models. As such any modeling assumption made will be associated with a generally undefined level of error when compared to the real world (Hirsch, 2007).

2.2 Defining the Discretization Process

Once the mathematical model is formulated we may begin the major process of translating or discretizing the geometrical domain and the set of governing differential equations making up the model into numbers that the computer recognizes.

The first action is to discretize the space defined by the edges, boundaries and domains of the geometry. This process consists of distributing points or finite elements like tets, bricks, prisms and pyramids (or any combination of these) to the space. This set of points, which replaces the continuity of the real space by a finite number of isolated points or elements in space, is called a grid or a mesh. As the whole objective of the simulation is for the computer to provide the numerical values of all the relevant variables, such as velocity, pressure, temperature, concentration and so forth, on these mesh points, it becomes clear that the outcome of the simulation and its accuracy can be extremely dependent on the grid properties and quality (Hirsch, 2007). As imperative programming languages like Fortran does not provide visual support this process requires expert knowledge beyond simple geometries.

After generating the mesh we may move on to the discretization of the model equations, which makes up the second branch of our modeling tree (Figure 2.1). Now as the computer only have access to the elements or points as defined in the mesh all mathematical operators such as the partial derivatives of the governing equations needs to be transformed into arithmetic operations on those same points in space (Hirsch, 2007). This conversion process from derivatives to arithmetic operations are the objective of various methods such as the finite element method, finite volume method, the boundary element method and so forth. In *COMSOL Multiphysics* several different methods are in use, but the emphasis is on the finite element method. Most critically though is that the method and additional configurations used are automatically chosen and tailored to the type of physics and geometry you are solving for. At the same time the user retains the option to manually adjust aspects of the discretization process like overriding the order of the elements used – that is if the shape of the elements are to be say linear or quadratic – on different components like velocity, pressure or temperature, which will affect the accuracy of the solution.

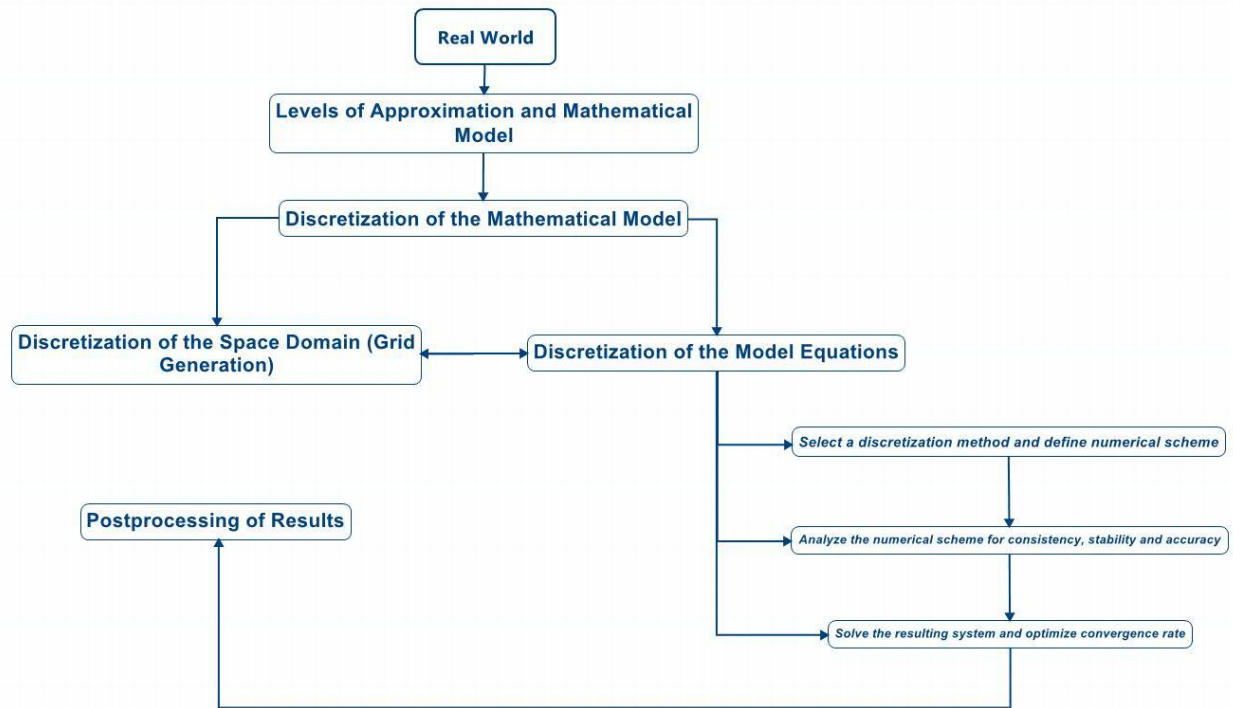


Figure 2.1 Modeling tree (Presented using XMind software, from (Hirsch, 2007))

2.3 Performing the Analysis Phase

Regardless of the discretization method that is being used the discretization process yields a set of algebraic relations between neighboring elements or points with one relation for each point. The final result is an algebraic system of equations that have as many equations as unknowns and is what makes up the numerical scheme. This numerical scheme then must satisfy a certain number of rules and conditions to be acceptable and subsequently it must be analyzed to establish the associated level of accuracy.

This phase of analyzing the scheme for consistency, stability and convergence are vital in the sense that any discretization will automatically generate errors as a consequence of the replacement of the continuum model by its discrete representation (Hirsch, 2007). This is true in a sense for both platforms – *COMSOL Multiphysics* and *Fortran* – but in the former extensive measures are already in place to secure that the various discrete representations is stable and accurate. The user is then left with the task of exercising judgment regarding the results of the simulation, and perform mesh refinement and validation procedures to ensure that the numerical scheme is in fact giving valid solutions. In the latter the researcher needs to be more intimately acquainted with the various numerical schemes available and their properties to find the most appropriate scheme for the envisaged application.

2.4 Defining the Resolution Phase

The last step in the discretization process is solving the numerical scheme to obtain the element or point values of the variables of interest. In *COMSOL Multiphysics* the software runs the analysis together with adaptive meshing (if selected) and error control using a variety of numerical solvers: direct and iterative sparse matrix solvers, algebraic and geometric multigrid methods, as well as a range of preconditioners. The direct linear system solvers computes the system matrix in one step and is as such computationally expensive, robust, and will benefit from shared memory parallelism. The iterative solver iterates until a relative tolerance is fulfilled, and uses various methods to divide the problem into a more coarse mesh, which it solves for, and then applies the solution to a finer mesh. As such the iterative solver requires less memory than the direct solver, but is less robust than its counterpart.

The solution is advanced by using either a segregated solver in which the solution variables are divided into subgroups that are solved for independently, or fully coupled solver, in which all the solution variables are solved for simultaneously for each iteration. As such the fully coupled solver is more computationally expensive than the segregated solver, but are more robust in terms of minimizing error. These are mutually exclusive and are a coupled to either a direct or iterative sparse matrix solver as shown in the chart below (Figure 2.2) which gives their relationships. These solution variables and matrix solvers works whether the problem is classified as stationary problem (steady-state) or as time-dependent problem (also called dynamic or unsteady problems). In the case of a stationary solver a damped Newton method is generally used, while for the implicit time-dependent schemes the BDF and generalized alpha stepping methods are available.

As was the case in the discretization process the software automatically chooses the appropriate settings based on the variables available, but the user retains the option to manually configure the settings. Moreover it automatically recognizes when multicore computing is available and reconfigures the solver settings accordingly. In *Fortran* the researcher would have to be acquainted with the solution algorithms available for the different classes of problems and would need to manually adjust these if say more physics was to be included in the model.

Once the solution is obtained, we have to manipulate this considerable amount of numbers to analyze and understand the computed variables. This can only be achieved through powerful visualization systems, which provide the software tools to study, qualitatively and quantitatively, the obtained results. This is true whether or not we use computational packages like *COMSOL Multiphysics* or imperative programming languages like *Fortran* but for the software these visualization systems comes as part of the package while in the latter you would

have direct access to the solution matrices and would have to manipulate these in some manner.

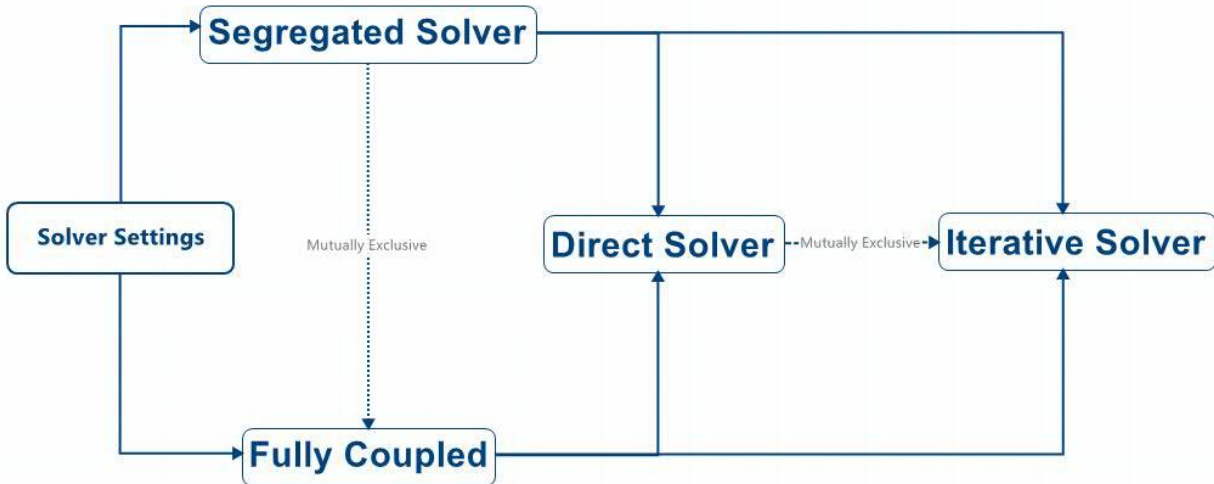


Figure 2.2 Solver settings (Presented using Xmind software)

2.5 Features of COMSOL Multiphysics

The software specific features of *COMSOL Multiphysics* is, given the scope of such computational packages, quite extensive. Here we will therefore limit ourselves to a general overview of the program together with some interesting facets as related to the current problem of designing a regenerative heat exchanger.

Addressing the general overview first we begin by noting that the user interact with the platform first and foremost through the *COMSOL Desktop* which provides an integrated environment with a unified workflow regardless of the application area. Here a *Model Tree* in a *Model Builder* gives the user full overview of the model and access to all functionality – geometry, mesh, physics settings, boundary conditions, studies, solvers, postprocessing and visualizations. Apart from noting that this environment lends itself for easy and general customization, a number of different application programming interfaces (APIs) are also available. Of these the *Livelink for MATLAB* interface are used for the development of the overall model in the current problem as it allows us to work with *COMSOL Multiphysics* in combination with the *MATLAB* technical computing language.

Aside from giving access to the core functionality and physics as described above the core platform may in addition be augmented by a number of add-on modules that can be

engaged for dedicated physics interfaces and tools like the *Heat Transfer Module*, and *Chemical Reaction Engineering Module* employed in this thesis. The interface modules under which the APIs falls comes as part of this extended functionality as well together with cross-platform integration with for example *Excel* and *AutoCAD* through *Livelink for Excel* and *Livelink for AutoCAD*, respectively.

The most interesting feature of *COMSOL Multiphysics* is perhaps that it comes with an in-built interpreter for mathematical expressions. This means that expressions including unknown field variables, their derivatives, spatial coordinates and time all can be assigned to variables for later use in for example boundary conditions, interpolation functions or in an analysis using the technical computing language of *MATLAB*. This means that most of the time there is no need to write code to adapt the software when there is need for a custom expression as we will see when constructing the numerical model.

CHAPTER 3

MATHEMATICAL MODEL

3.1 Geometry

The transport equations and fluid-structure interactions is in the present thesis analyzed by considering the sinusoidal channel as shown below (Figure 3.1). The basic equations governing the shape of a single channel is the sinusoidal function,

$$y = a \cdot [1 - \cos(\frac{\pi}{b} x)], \quad (3.1)$$

where a is the half-height of the sine duct and b is the half-width of the duct, and a lower (or upper) boundary that is simply given as a flat plane.

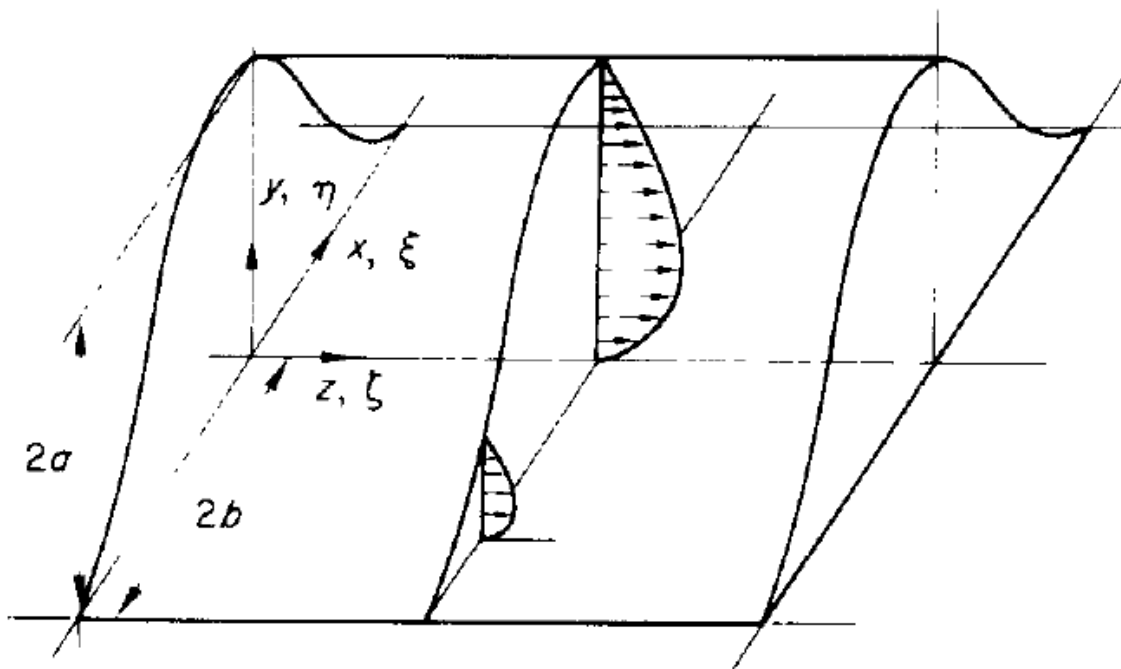


Figure 3.1 Conceptual drawing of the sine channel with fully developed flow (From Sherony & Solbrig, 1970).

From this conceptual drawing we note the flow will be symmetrical around the centerline of the air stream and as such it is only necessary to solve the variables of interest for

half of the channel. On the other hand the flow will not be symmetrical across the sine and neither on the lower boundary because of the honeycombed matrix structure in which the sine channels are stacked on top of each other. There will however exist skew-symmetry across all of these boundaries and as such we are left with a few options regarding how to define the geometry. We could consider the air streams on both sides of the sine or we could use the skew-symmetry to find the appropriate boundary conditions on the sine wall from the adjacent air stream. In any case we would still need to impose skew-symmetry boundary conditions on the flat boundaries to restrict the problem. As simulating both air streams would necessarily be more computationally expensive, and as we still need to define the other skew-symmetry conditions the latter alternative where we in addition would need to define the symmetry across the sine is considered the most efficient option.

Apart from these considerations the conceptual drawing also reveals why a two-dimensional representation of the channel will fail to capture any transverse influences as there isn't any symmetry across the channel in the x and y (or angular) direction. A two-dimensional model will therefore necessarily carry a hydraulic diameter that is simply based on infinite parallel plates, and a corresponding flow field that at best makes for a weak approximation of the actual flow at any given x or y (or angular) coordinate. This is further illustrated from the fully developed velocity profile in the drawing where the maximum velocity is indeterminate and could never be replicated in any other reduced formulation. As such a one-dimensional representation will inherit far fewer complications than a two-dimensional one as the hydraulic diameter doesn't discriminate between different geometries, but at the same time it carries no information on how the equations governing the local diffusional processes behaves.

The exceedingly complex three dimensional formulation will therefore be the focus of this thesis and our attention will be directed towards the features observed in the sine geometry. Still it is recognized that a two-dimensional model, while expected to be inaccurate, provides an excellent tool to gain a clearer understanding of how the physics works and verify that the governing equations indeed behave as expected before launching on a three-dimensional campaign.

3.2 Assumptions

In this thesis the numerical model solves the equations governing the velocity, temperature and concentration fields in a single air stream, together with the temperature of the sine-shaped matrix, and the convective heat fluxes between the matrix walls and air streams. So while this model uses an untreated clean aluminum structure that doesn't support sorption processes as a mode for mass transfer it still solves for the water vapor present in the air. The channels themselves are cyclically being exposed to two physically separated flows (of which the air streams originate) as the rotary matrix, of which they make up a small fraction, spins

around its own axis with constant angular velocity. As such, the formulation is three-dimensional and transient, with space (x, y, z) and time (t) as the independent variables.

The idealizations setting the stage for the model analyzed in this thesis is given below.

1. Body forces such as gravity, centrifugal, Coriolis, and electromagnetic do not exist.
2. Radiation effects are negligible compared to heat transfer by convection as a result of low temperatures.
3. Thermal energy sources, viscous dissipation effects, and flow work within the fluid are neglected.
4. No free convection, mass diffusion, chemical reaction, change of phase, and electromagnetic effects takes place.
5. The velocity distribution of the air are independent of the fluid temperature.
6. The channels are equal and uniformly distributed throughout the wheel.
7. The state properties of each inlet stream are uniform radially (r-direction), but may vary with time (or rotational angle).
8. Heat (and mass transfer) from the exchanger to the surroundings (besides the channel inflow and outflow) are negligible.
9. The velocity, temperature and concentration profiles develop simultaneously within each channel.
10. Pressure drop in the axial flow are negligible with respect to the total pressure.
11. The convective heat transfer between the air streams and the matrix surface can be evaluated by employing bulk properties and film coefficients.
12. The dependent variables and properties vary periodically with time each rotation of the wheel (i.e., within one cycle the dependent variables and properties vary in a cyclic manner).

We note that these assumptions are generally comparable with those presented in the literature in that many are dedicated to permit the channels to be independently treated, to provide a uniformly distributed transfer area, to ensure constant mass flow rate of dry air for all channels and to allow energy balances to be written (Tunaa, 2013). The simplifying assumptions that make up the basis for the present study are however more general than those given in the literature and in what follows we will look into some of these differences. For a more detailed analysis of the implications of the above idealizations as well as other commonly used assumptions in the literature the reader is referred to e.g. Tunaa (2013).

As noted previously the present model is not limited to a one-dimensional analysis of the air as was the case in the investigations by Simonson and Besant (1997) and Sphaier and Worek (2004), examined in Tunaa (2013). This allows for an view of how the velocity, temperature and concentration profiles is expected to develop and allows for the analysis of

how various influences will affect not only the bulk properties found in other studies but also local properties which may be of importance.

On the other hand the present investigation does not include mass transfer through sorption nor condensation and as such does not enable the study of how the separated flows interact through these important modes of transfer. Furthermore any modifications made to the model in order to incorporate such effects would need additional assumptions along the lines of those presented in the literature (c.f. Tunaa, 2013).

Another important assumption that is relaxed in this thesis compared to previous studies is the requirement that all surfaces perpendicular to the air stream is adiabatic. Instead symmetry is imposed appropriately around the channel walls to reflect the presence of the air streams in the adjacent channels.

3.3 Conservation of Mass and Force Balances (Momentum Equations)

As the model analyzed in this paper is three-dimensional it becomes necessary to solve the momentum equations in order to establish a flow field on which the transport equations for heat transfer considered later forms an intimate relationship with. To bridge the gap between what simplifying assumptions are made in the current model and those that are usually made in regard to laminar flow through ducts, it is prudent to take a look at these in turn. We start by giving the complete set of continuity and momentum equations,

$$\frac{\delta \rho}{\delta t} + \nabla \cdot (\rho \mathbf{u}) = 0 \quad (3.2)$$

$$\rho \frac{\delta \mathbf{u}}{\delta t} + \rho (\mathbf{u} \cdot \nabla) \mathbf{u} = \nabla \cdot [-p \mathbf{I} + \mu (\nabla \mathbf{u} + (\nabla \mathbf{u})^T) - \frac{2}{3} \mu (\nabla \cdot \mathbf{u}) \mathbf{I}] + \mathbf{F} \quad (3.1)$$

where

- ρ is the density (kg / m^3)
- \mathbf{u} is the velocity vector (m / s)
- p is the pressure (Pa)
- μ is the dynamic viscosity ($N \cdot s / m^2$)
- \mathbf{F} is the volume force vector (N / m^3)

The most commonly invoked assumption for flow geometry in ducts or forced convection in general is that the velocity profile may be assumed independent of the heat or mass transfer processes occurring. This involves considering the flow properties as constant, and hence density changes due to temperature and concentration variations may be neglected.

The flow in this case is described as being incompressible or as constant-density flow. The preceding two principles – mass conservation plus three force balances – are thus sufficient for solving the flow part of the convective heat transfer problem. We note at this juncture the availability of four equations for determining four unknowns (three velocity components plus pressure). Moreover with the flow independent of the unsteady state heat or mass transfer problem, all unsteady state terms in the continuity and momentum equations may be neglected (Sherony & Solbrig, 1970).

Another assumption that is almost always applied with regard to flow geometry in ducts in regard to convective heat transfer is that body forces such as gravity, centrifugal, Coriolis, and electromagnetic do not exist. This simplifies the analysis as the volume force vector vanishes in all three force balances (Shah and London, 1978).

From here studies of flow geometry in ducts diverge in two subcategories – one that consider only the fully developed flow region and one that in addition describes the hydrodynamic entrance region where the velocity boundary layer is developing. Here we are interested in the latter as the model considers simultaneously developing flow, but as the developed region makes up the greater part of the flow length the most important features can be gleaned from such analysis.

In fact only the fully developed laminar flow (and heat transfer problem) for sine ducts has been investigated to the author's knowledge. The equations analyzed in such situations are simplified by recognizing that for fully developed flow the velocities perpendicular to the flow direction, u and v , are zero. The continuity equation then reduces to the statement that the axial change in velocity, w , are zero. Utilizing the above assumptions and the continuity equation the x and y momentum equations reduces to a statement that the transversal pressure gradients are zero while the governing boundary layer type z momentum equation becomes,

$$\mu \left(\frac{\partial^2 w}{\partial x^2} + \frac{\partial^2 w}{\partial y^2} \right) = \frac{\delta p}{\delta z} \quad (3.2)$$

These equations implies that the pressure drop in the axial direction is constant (Sherony & Solbrig, 1970). We also note that since the continuity equation is utilized in deriving the momentum equations only the solution to the momentum equation is required for the fully developed laminar fluid flow problem. Only the no-slip condition at the boundary is thus needed to close the problem and the equations can be readily solved using a numerical method such as a finite-difference method as in Sherony and Solbrig (1970) or as a least-square method as in Shah (1975).

For the hydrodynamic entrance flow problem however, where the velocity boundary layer is developing, these assumptions are no longer valid. In fact the flow problem can now no longer be classified as strictly a boundary layer problem. This is because very near the entrance the axial molecular momentum transport $\mu(\partial^2 u / \partial x^2)$ is not a negligible quantity, and far from the entrance, the boundary layer thickness is not negligible compared to the characteristic dimension of the duct (Shah and London, 1978). In addition it is also conceivable that very close to the entry the transverse pressure gradient across the section may not be negligible.

To overcome these difficulties it is customary to simply assume that those quantities are negligible and that the Prandtl boundary layer idealizations,

$$w \gg u, v \quad (3.3)$$

$$\frac{\delta w}{\delta x}, \frac{\delta w}{\delta y} \gg \frac{\delta w}{\delta z}, \frac{\delta u}{\delta x}, \frac{\delta u}{\delta y}, \frac{\delta u}{\delta z}, \frac{\delta v}{\delta x}, \frac{\delta v}{\delta y}, \frac{\delta v}{\delta z} \quad (3.4)$$

even though not strictly applicable to the entrance flow problem remains good approximations for laminar flow in ducts. The terms of the x and y momentum equations are then found to be one order of magnitude smaller than the corresponding terms of the z momentum equation and hence may be neglected. This implies that the pressure drop is a function of the axial coordinate z only, and that if we invoke the idealizations made for the fully developed flow, the governing boundary layer type z momentum equation becomes,

$$\rho \left(u \frac{\delta w}{\delta x} + v \frac{\delta w}{\delta y} + w \frac{\delta w}{\delta z} \right) = - \frac{dp}{dz} + \mu \left(\frac{\partial^2 w}{\partial x^2} + \frac{\partial^2 w}{\partial y^2} \right) \quad (3.5)$$

There is again imposed a no-slip condition on the boundary, but we now also require an initial condition, which is usually a uniform velocity profile at the entrance, and that the continuity equation be solved simultaneously.

The system of equations describing the flow problem in the case of nonsymmetrical ducts such as the sine configuration has four unknowns $-(u, v, w)$ and (p) , but only two equations so that two additional equations are needed to close the system. A third equation in addition to the momentum and continuity equations are thus needed to describe the behavior of the u and v components in the entrance region. Such an equation for the sine configuration is not known to the author. Finally the axial pressure distribution has to be obtained from another physical constraint such as from the solution of the mechanical energy integral equation.

In the model investigated in this paper we use the single-phase laminar flow branch in the *Computational Fluid Dynamics (CFD) Module* of the *COMSOL Multiphysics* software package. This module has predefined physics that enables us to solve for the full momentum equations as defined in equation (3.1) given at the beginning of this chapter. As detailed above it makes sense to assume that the flow geometry is independent of the temperature and concentration problem and that body forces exerts a negligible influence on the air stream. These simplifications are therefore retained here and can be exercised by selecting for incompressible flow and noting that by default no body forces are included. The resulting system of equations used in the present model to simulate fluid flow thus becomes,

$$\rho(\mathbf{u} \cdot \nabla)\mathbf{u} = \nabla \cdot \left[-p\mathbf{I} + \mu(\nabla\mathbf{u} + (\nabla\mathbf{u})^T) \right] \quad (3.6)$$

$$\rho(\nabla \cdot \mathbf{u}) = 0 \quad (3.7)$$

The no-slip boundary condition for this case is,

$$u, v, w = 0 \quad \text{on } \Gamma \quad (3.8)$$

The initial condition is a uniform velocity profile at the entrance or sufficiently upstream of the exchanger (to be explained later),

$$w = w_{avg} \quad \text{at } z = 0 \quad \text{or} \quad w = w_{face} \quad \text{at } z < 0 \quad (3.9)$$

At the outlet a boundary condition that specifies vanishing viscous stress along with a Dirichlet condition on the pressure is used as it admits total control of the pressure level along the entire boundary,

$$\mu(\nabla\mathbf{u} + (\nabla\mathbf{u})^T)\mathbf{n} = 0, \quad p = p_0 \quad (3.10)$$

As is evident from the discussion above this will include quite laborious computations as all the terms previously considered negligible now are solved for. In a sense we might be sacrificing computational resources to include effects that may have a negligible influence on the heat transfer problem, but given the assumptions above this is largely redeemed by the fact that we only have to solve for the flow geometry once. From the discussion above we also learned that no investigation has been performed to include the hydrodynamic entrance region in the simplified scheme outlined above as a result of difficulties in closing the problem. As such there is no alternative to the above formulation while at the same time we have no means of verifying the resulting developing velocity profile.

3.4 First Law of Thermodynamics

The heat transfer part of the convection problem requires a solution to the temperature distribution throughout the flow. For laminar forced convection in which the solid walls of the duct guides the heat-carrying fluid stream this means determining the fluid and wall temperature distributions and the heat transfer rate between the wall and fluid. Such a problem has mathematically complex features, such as heat conduction in normal, peripheral and axial directions; variable heat transfer coefficients along the periphery and in the axial direction; and changing velocity and temperature profiles along the flow length (Shah and London, 1978).

The sine configuration with its high-conductivity matrix walls clearly exhibits most of these complicating features as we will go into detail later on and the current problem are therefore classified as a conjugated problem as opposed to a conventional convection problem (c.f. (Bejan, 2004)). The first step in analyzing this class of problem is to recognize that we need to consider the temperature and heat fluxes as continuous functions at the solid wall-fluid interface while solving for the energy equations (or first law of thermodynamics) simultaneously.

3.4.1 Conjugated Heat Transfer Problem

The formulation of the scalar energy equation for the air stream and wall are in the present analysis simplified according to the assumptions made before. To reiterate thermal energy sources, viscous dissipation effects, and flow work within the air stream are neglected. In the absence of radiation, free convection, mass diffusion, chemical reaction, change of phase, and electromagnetic effects, the governing differential equations and boundary conditions can be written as follows.

Transport Phenomena in Air Stream

$$\underbrace{\rho C_p \frac{\delta T}{\delta t}}_{\text{rate of energy accumulation}} + \underbrace{\rho C_p \mathbf{u} \cdot \nabla T}_{\text{net transfer of energy by fluid flow}} = \underbrace{-\nabla \cdot \mathbf{q} = \nabla \cdot (k \nabla T)}_{\text{net heat transfer by conduction}} \quad (3.11)$$

where

- ρ is the mixture density (kg/m^3)
- C_p is the mixture specific heat capacity at constant pressure (J/kgK)
- T is the absolute temperature (K)
- \mathbf{u} is the velocity vector (m/s)
- \mathbf{q} is the conduction heat flux vector (W/m^2)

- k is the mixture thermal conductivity (W/m^2K)

subject to the boundary conditions,

$$T = T_{wall} \quad \text{on } \Gamma \quad (3.12)$$

$$-\mathbf{n} \cdot (-k\nabla T)_{air} = -\mathbf{n} \cdot (-k\nabla T)_{wall} \quad \text{on } \Gamma \quad (3.13)$$

and initial condition,

$$T = T_o \quad \text{at } z = 0 \text{ (or } z = L) \quad (3.14)$$

Transport Phenomena in Matrix

$$\underbrace{\rho C_p \frac{\delta T_{wall}}{\delta t}}_{\text{rate of energy accumulation}} = \underbrace{-\nabla \cdot \mathbf{q} = \nabla \cdot (k\nabla T_{wall})}_{\text{net heat transfer by conduction}} \quad (3.15)$$

where

- ρ is the matrix density (kg/m^3)
- C_p is the matrix specific heat capacity at constant pressure (J/kgK)
- T_{wall} is the absolute temperature (K)
- \mathbf{q} is the conduction heat flux vector
- k is the matrix thermal conductivity (W/m^2K)

subject to the boundary conditions,

$$-\mathbf{n} \cdot (-k\nabla T)_{wall} = 0 \quad \text{at } z = 0, L \quad (3.16)$$

$$q' \text{ on shared boundaries are skew-symmetric with adjacent channels} \quad (3.17)$$

As can be seen, the energy equations for the air stream and matrix are coupled by the boundary conditions of equations (3.11) and (3.12). Moreover as the channel is not isolated but instead surrounded by adjacent channels (c.f. Fig. 1.1) the heat flux over shared boundaries from the accompanying air streams needs to be taken into account. These air streams are presumably identical to the air stream in the channel solved for and from the matrix arrangement and flow geometry we observe that the heat flux on shared boundaries has to act in a skew-symmetric manner to the heat flux observed on the inside of the channel. It should also be noted that as a consequence of the continuous solid wall-fluid interaction along the

entire length of the channel the temperature profile is always variant (never fully developed) for the family of problems that this formulation subscribes too (Shah and London, 1978).

The conjugated problem as formulated above may be realized in a number of ways by synthesizing different interfaces of the core physics platform and/or the *Heat Transfer Module*. As we've already assumed that the flow geometry can be solved independently from the temperature problem and that the unsteady terms vanishes the usefulness of the *Conjugated Heat Transfer* interface is diminished. The energy balance for the air stream will therefore be represented by the *Heat Transfer in Fluids* interface which by default gives equation (1.10) . The temperature problem for the matrix wall may be solved using the *Heat Transfer in Solids* interface which gives equation (1.14) by default or by using the *Heat Transfer in Thin Shells* interface which gives a slightly modified version of equation (1.14),

$$\rho d_s C_p \frac{\delta T_{wall}}{\delta t} + \nabla_T \cdot (-d_s k \nabla_T T_{wall}) = Q_{oop} \quad (3.18)$$

where ∇_T is the tangential derivative along the shell, and

- d_s is the shell thickness (mm)
- Q_{oop} is the out-of-plane heat flux

3.4.2 Thermal Boundary Condition

The thermal boundary condition is the set of specifications describing the temperature and/or heat flux conditions at the inside wall of the duct. Obviously there are a large variety of thermal boundary conditions that may be specified for the temperature problem as discussed above, and the heat transfer flux of flows operating in the laminar regimes is strongly dependent on the condition that is being used (Shah and London, 1978). Paired with the observation that these imposed conditions may to varying degrees apply for the actual physics the engineering objective of choosing the appropriate conditions is not straight-forward and is often compromised by the availability of data.

To find the thermal boundary condition most applicable to the current model it is helpful to think in terms of the classes of thermal boundary conditions as systemized and defined by Shah and London (1978). These are the thermal boundary conditions of approximately constant axial wall temperature (T) and approximately constant axial wall heat flux (H), respectively.

We can easily discard the notion of approximately constant axial wall temperature under normal operating conditions by noting that the hydraulic diameter is very small

compared to the length of the channel and so if a temperature differential exists between the supply and exhaust air streams it will manifest itself in varying axial matrix temperature.

The thermal boundary condition of approximately constant axial wall heat flux per unit length is however realized in the channel and variations of this theme based on the duct geometrical properties and thermal conductivities is what is generally applied to heat exchangers (Shah and London, 1978). In the thin high-conductivity matrix analyzed in this paper the temperature across any cross section may be taken as uniform and the peripheral heat conduction may be idealized to be infinite. This is equivalent to idealizing zero wall thermal resistance in the normal and peripheral directions and coupled together with the assumption of zero axial heat conduction we then have the (HI) boundary condition:

$$q' = \dot{m}C_p \frac{\delta T_b}{\delta z} = \text{constant}, \quad \text{independent of } z \quad (3.19)$$

$$T|_{\Gamma} = T_{\text{wall},m} = T_{\text{wall}} = \text{constant}, \quad \text{independent of } (x, y) \quad (3.20)$$

where the fluid bulk mean temperature and mean peripheral wall temperature are defined as,

$$T_{\text{wall},m} = \frac{1}{P} \int_{\Gamma} T_{\text{wall}} ds \quad (3.21)$$

$$T_b = \frac{1}{A_c w_b} \int w T dA_c \quad (3.22)$$

This formulation is mathematically amenable and consequently it is the most frequently investigated boundary condition in the literature. It should be noted however that in practice it may be difficult to achieve this boundary condition for noncircular ducts with corners and variable peripheral curvature. The underlying reason for this is easiest to conceptualize when thinking of the heat carrying fluid stream and its highly variable flow geometry with a high-velocity core at a location that cannot be predicted analytically (Shah and London, 1978) and near stagnant regions near the corners. The flow geometry in these regions will interact with the matrix wall according to the local environment and it is therefore unlikely that the geometry of the channel will not cause some peripheral variation of the temperature. Nonetheless it remains a good approximation by virtue of the high conductivity of the matrix material.

A consequence of the uniform (or near uniform) wall temperature around the noncircular periphery of the channel is in any case inevitably that the local heat flux is variable around the periphery to accommodate the flow geometry. In particular it will vary from a maximum in wall regions close to the stream to a minimum in wall regions close to other wall

regions (q'' drops to zero in the sharp corners of the cross section) (Bejan, 2004). Thus q' is perimeter line integral of the local peripheral wall heat fluxes q'' , related as follows,

$$\frac{q'}{P} = q''_{avg} = \frac{1}{P} \int_{\Gamma} q'' ds \quad (3.23)$$

In turn the local peripheral wall heat flux at a point on the boundary (and indeed the peripheral average) are given in terms of the operationally convenient heat transfer coefficient h , sometimes called the convective conductance, and the temperature difference ($T_{wall} - T_b$) as,

$$q''_p = h_p (T_{wall} - T_b) = Nu_p \frac{k}{D_h} (T_{wall} - T_b), \quad Nu_p = \frac{h_p}{k/D_h} \quad (3.24)$$

Also written as part of this balance are the non-dimensional Nusselt number Nu which can be deduced by normalizing the convective conductance h to the pure molecular thermal conductance k/D_h .

As q'' varies along the perimeter, the heat transfer coefficient follows suit and varies too. As such the Nusselt numbers listed in the literature (c.f. (Shah & London, 1978)) refer to the heat transfer coefficient averaged over the duct perimeter. Information about the local peripheral values are generally not available in the literature except for a few select configurations and this presents a problem as we're interested in local temperatures in the channel. A major part of the numerical implementation of the mathematical model is therefore to define the local peripheral values from the known averaged peripheral values.

It should be noted that the equality on the left of equation (1.17) represents an energy balance in the absence of axial heat conduction within the fluid (together with the assumptions provided earlier), but also one that is void of axial heat conduction in the wall. The absence of axial heat conduction within the fluid presumably makes for a good assumption as long as its magnitude is negligible compared to advection. Depending on the temperature potential between the air streams however the wall axial heat conduction is likely to play an important role in conveying heat upstream to further enhance convection. This may or may not adversely affect the legitimacy of using the Nusselt numbers calculated without including such effects as wall axial heat conduction is included in the model.

3.5 Mass Conservation of Constituents in the Air Stream

In the previous discussion on momentum equations we made the assumption that the flow was constant-density in order to procure the flow geometry. The centerpiece of the analysis was the principle of continuity through the control volume and we invoked it on the

case of a fluid of density ρ whose composition was not questioned. However the air stream under consideration is moist air, a mixture of dry air and water vapor, and in this section we will apply the principle of mass conservation on each of those constituents.

As we now are interested in how the density or concentration field changes in the air stream in response to the heating (or cooling) by the matrix, as opposed to obtaining the flow geometry, the unsteady transient terms associated with mass transfer can no longer be neglected for the constituents. In the absence of change of phase, chemical reactions, sorption and migration caused by an electric field the governing differential equations and boundary conditions may be written as follows.

$$\rho \frac{\delta w_i}{\delta t} + \rho(\mathbf{u} \cdot \nabla)w_i = -\nabla \cdot \mathbf{j}_i = \nabla \cdot \left(\rho D \nabla w_i + \rho w_i D \frac{\nabla M_n}{M_n} \right), \quad (3.25)$$

$$M_n = \left(\sum_i \frac{w_i}{M_i} \right)^{-1}, \quad \mathbf{N}_i = \mathbf{j}_i + \rho \mathbf{u} w_i, \quad i = a, vw$$

where,

- ρ is the mixture density (kg / m^3)
- w_i is the mass fraction of constituent i (kg / kg)
- \mathbf{u} is the velocity vector (m / s)
- \mathbf{j}_i is the fickian diffusion flux vector
- D is the mass diffusivity (m^2 / s)
- M_i is molecular weight of constituent i ($kg / kmol$)

subject to the boundary condition,

$$-\mathbf{n} \cdot \mathbf{N}_i = 0 \quad \text{on } \Gamma \quad (3.26)$$

and initial condition,

$$w_i = w_{o,i} \quad \text{at } z = 0 \text{ (or } z = L) \quad (3.27)$$

The mass transfer problem is coupled to the heat transfer problem in that the mass diffusivity, whose units is m^2/s , is a transport property whose numerical value depends on the mixture pressure, temperature and composition. In turn the thermodynamics properties of the air stream are defined as a function of the quantity of vapor in the moist air which the concentration equation (3.27) solves for. As observed the diffusion flux vector is assumed to be

governed by Fick's law of mass diffusion in the air stream as is appropriate when molecular diffusion is not the dominating transport mechanism.

Given the proportionality that links molar concentration and mass fraction as a means of quantizing composition, defined by the following relation,

$$c = \frac{\rho w}{M} \quad (3.28)$$

the concentration equation formulated above can be replaced with a governing equation written in terms of molar concentration,

$$\begin{aligned} \frac{\delta c}{\delta t} + \mathbf{u} \cdot \nabla c &= -\nabla \cdot \mathbf{j} = \nabla \cdot (D \nabla c), \\ \mathbf{N} &= \mathbf{j} + \mathbf{u}c \end{aligned} \quad (3.29)$$

where,

- c is the molar concentration of water vapor (mol / m^3)
- \mathbf{j} is the fickian diffusion flux vector
- D is the mass diffusivity (m^2/s)

subject to the boundary condition,

$$-\mathbf{n} \cdot \mathbf{N}_i = 0 \quad \text{on } \Gamma \quad (3.30)$$

and initial condition,

$$c = c_o \quad \text{at } z = 0 \text{ (or } z = L) \quad (3.31)$$

It should be noted that this formulation only is valid if the gas mixture can be considered dilute. This is true in the case of moist air, where the species of interest, water vapor, acts a dilute solute in the solvent dry air. As such the above formulation in terms of molar concentration provides an alternative to the mass fraction formulation if desired. The above formulations may be implemented using either the *Transport of Concentrated Species* or *Transport of Diluted Species* interfaces, respectively, of the *Chemical Reaction Engineering Module*.

3.6 Conjugated Heat and Mass Transfer Problem

The conjugated heat transfer problem and mass conservation of constituents in the air stream as formulated above together with momentum equations solves for velocity, temperature and concentration field in what is known as a heat wheel or regenerative heat

exchanger. It allows us to find hot or cold spots locally within the channel and can be used as a tool to predict when conditions are in place for condensation to occur. To build a numerical model that performs that multiphysics simulation for us is the objective of the next chapter.

At the same time it may be of equal interest to point out what the system of equations as described in the previous sections does not include to further our understanding of the limitations of the current formulation. The most obvious simplifying feature is that the concentration equation in its present state of zero mass flux on the mass flux boundaries does not allow for neither sorption nor condensation. As such the bulk water vapor partial pressure in the axial direction is expected to be conserved and equal to the water vapor partial pressure of the inflow air stream, while there will be what amounts to negligible gradients in the transversal directions as a result of isotropic mass diffusion. From moist air theory (see Appendix A) then the relative humidity $\phi = p_v / p_{sat}$ is a function of the saturation pressure of water vapor only which in turn is dependent on the local temperature.

Now if we were to coat the matrix walls with a desiccant like silica gel or molecular sieve, each with their own set of characteristics, we would have to consider mass transfer by sorption processes. The mass flux on the wall-fluid interface may in the case of sorption mass transfer be defined in similar terms as the heat flux of the temperature problem because of the symmetry between the mass transfer scaling laws and their heat transfer correspondents (Bejan, 2004). More specifically we can define a convective mass transfer coefficient h_m based on the difference between the species concentration of the exposed side of the desiccant $\rho_{d,s}$ and the bulk concentration of the stream ρ_b . The local peripheral rate of species (water vapor) exchange between the air stream and the desiccant could then be given as,

$$\dot{m}_p'' = h_{m,p} (\rho_{v,s} - \rho_b) \quad (3.32)$$

The engineering objective would then be to find the convective mass transfer coefficient and the species concentration on the surface of the desiccant. The latter will of course be dependent of the moisture content and temperature of the desiccant and could be found using either sorption isotherms as in Simonson and Besant (1997) and Bilodeau et al. (1999) or by considering local diffusional processes within the desiccant (or sorbent felt) as in Sphaier and Worek (2004). Either way we would not only need to consider the mass conservation of water vapor in the air stream as in the concentration equations (3.25-3.27) but also a similar set of equations for the mass conservation in the desiccant (or sorbent felt). This would include the rate of water vapor increase in the control volume (a storage term) and rate of water vapor transfer into the control volume.

With that in mind it is clear that the problem now indeed has to be classified as a conjugated heat and mass transfer problem in that the water vapor exchange between the desiccant and the air stream will necessarily be accompanied by heat transfer as well. In particular when moisture is adsorbed on the matrix, heat is released (adsorption is exothermic) and the local temperature of the air and matrix is increased. In the same manner the desorption of moisture into the air stream serves to decrease the local temperature (desorption is endothermic) of the air and matrix. This means that if the heat and moisture transfer is in the same direction between the supply and exhaust air (which is the case under normal winter operating conditions) the warmer of the two inlet streams (the humid exhaust air) is simultaneously cooled and dried and the cooler air stream (the cold dry supply air) is heated and humidified (Tunaa, 2013). In regard to our previous discussion on the relative humidity being a function of the saturation pressure of water vapor only (as for the heat wheel) this is clearly no longer the case when sorption is considered as now the mass fraction (and consequently the water vapor partial pressure) will change in response to the mass transfer.

Whether we consider a heat wheel or a heat wheel coated with an desiccant (an energy wheel) condensate will start to precipitate out of the exhaust air if the air temperature adjacent to the surface falls below its local dew-point temperature. For heat wheels the dew point of interest is simply that of the incoming air stream as no water is precipitated out of the air unless it becomes saturated. On a Mollier chart this change in the state of the exhaust air takes place along a line of constant water vapor content (c.f. Figure 1.2a and Appendix A) and leads to states of higher relative humidity with declining temperature. In energy wheels the dew point will gradually decrease as the warm and humid exhaust air flows through the channels and gives off water to the desiccant. As the exhaust air is simultaneously cooled down by the matrix however the relative humidity will still increase provided that the supply temperature is sufficiently low (c.f. Figure 1.2b).

In any case if at some point along the rotor depth the exhaust air is sufficiently cooled down (to its dew point) then the relative humidity will be unity (i.e. $\phi = 1$), the water vapor in the air is saturated and condensate will start to form on the rotor surface. In a heat wheel this condensate will form as a thin film of water whereas for an energy wheel this additional moisture will simply be collected by the desiccant, which has large moisture retention capacity and can often hold its equivalent mass in water before water begins to run off (Simonson, 1998). As the rotor rotates, this condensate will then be transferred to the supply side where it will be evaporated. The mode of moisture transfer under saturated conditions is thus in the form of a condensation/evaporation cycle (or ablimation/sublimation at temperatures below the triple point). The danger in regard to condensation or frosting is thus if the supply air becomes saturated at the entrance (the dew point will continuously increase as the cold air is

heated up) leaving behind a zone in which the condensate/frost can continuously build up with each consecutive rotation.

To summarize the processes of sorption and condensation can both be modeled by introducing a mass transfer term like (3.32) in the case of sorption ($\varphi < 1$) or a similar term accounting for the rate of phase change when the air is saturated and thus limited to $\varphi = 1$, to the concentration equations of (3.25-3.27). As discussed above the treatment of the heat wheel and energy wheel will be different (with the energy wheel requiring additional equations) but in any case the moisture transfer leads to accompanying heat transfer which needs to be accounted for in the temperature problem of the air stream and the matrix of equations (3.11-3.14) and (3.15-3.16), respectively. For a more thorough discussion on the nature of the sorption mechanism and the mechanisms behind condensation (and frosting) including their consequences on the wheel operation, the reader is referred to Tunaa (2013).

The limitations of the present analysis is thus revealed in that even if we do not consider sorption we have no mechanism by which the amount of condensate that precipitates out of the exhaust air stream is accounted for (and by extension the accompanying heat transfer), and so even in the event of condensation the condensate will not be transferred to the supply air stream. As such this analysis can only evaluate when there will be a danger of sustained condensate in the supply section along with the length of this zone by pinpointing the zone of condensation is along the flow axis in the exhaust sector of the wheel.

CHAPTER 4

NUMERICAL MODEL

4.1 Defining the Global Parameters

We begin the process of constructing the numerical model from the mathematical formulation by providing the model parameters needed for the simulation. The relevant parameters along with some typical values are given in Table 4.1. This includes the geometrical dimensions of the single sine channel, namely the half height and half width of the duct and the thickness of the wall together with the channel length. Next operational parameters like the mass flow, temperature and relative humidity are in place to control the flow characteristics. Together with the wheel diameter these can be used in accordance with moist air theory to produce the density and velocity at the inlets. Also listed is the applied time for the supply and exhaust air streams, which are assumed to be identical in this paper. This corresponds to equal wheel sections for the opposing streams and in a scenario where this is no longer true the applied time would differ. In addition the mass diffusivity of the binary gaseous mixture of air-water vapor has been defined at atmospheric pressure and a temperature of 298 K (Bejan, 2004). This value can then subsequently be extrapolated to temperatures and pressures that differ from that specified in the table by exploiting an experimental formula knitting them together.

A primary objective of this numerical model has been that the entire model should be controlled by these parameters and that the subsequent geometry, definitions, variables and so forth should be defined in terms of the parameters listed here. As such any change in any of these will directly translate into those being automatically adjusted and recalculated to reflect that change. The only exception to this is the thermal boundary condition used which will in part depend on the matrix material and so the averaged peripheral Nusselt numbers will always need to be manually redefined.

4.2 Defining the Sine Geometry

The sine channel may be constructed in a number of different ways and may either be native to the *COMSOL Kernel* or imported from more specialized CAD software. In this paper it has been built using the *COMSOL Kernel* in accordance with the objective of controlling the entire process using the model parameters. Below you can view the cross section along with the geometrical functions used with the innermost sine curve displayed (Parametric Curve 1) (Figure 4.1).

Table 4.1 Input data used in simulations

Name	Expression	Value	Description
a	$(1/2)*1.5[\text{mm}]$	7.5000E-4 m	Half height of the sine duct
b	$(1/2)*3.0[\text{mm}]$	0.0015000 m	Half width of the sine duct
Rwall	0.04[mm]	4.0000E-5 m	Wall thickness
L	100[mm]	0.10000 m	Channel length
D_wheel	0.9[m]	0.90000 m	Wheel diameter
A_frontal	$\pi*(D_wheel/2)^2$	0.63617 m ²	Wheel frontal area
T_supply	-10[degC]	263.15 K	Supply temperature
T_exhaust	20[degC]	293.15 K	Exhaust temperature
phi_supply	0.2	0.20000	Supply relative humidity
phi_exha...	0.4	0.40000	Exhaust relative humidity
m_supply	0.5[kg/s]	0.50000 kg/s	Supply mass flow
m_exhaust	0.5[kg/s]	0.50000 kg/s	Exhaust mass flow
t0	0[s]	0 s	Initial time
period	1.5[s]	1.5000 s	Applied time
dt	period/3	0.50000 s	Output time step
tf	t0+period	1.5000 s	Final time

The approach used here is to define two parametric curves that is given by the sinusoidal function of eq. (3.1) and that are separated by the wall thickness. The sinusoidal function is recognized in the expression field below (Figure 4.1) together with appropriate parameters and positioning. Next a series of straight lines defined by linear Bézier Polygons were placed appropriately to build the lower arc, smoothing out remaining portions of the upper sine to secure correct skew-symmetry and otherwise completing the cross section. Then in order to prepare for extruding the cross section to its appropriate length and to be able to define the domain and boundaries of the physics, the air stream and matrix wall were made solid. These functions and conversions are seen below under the plane geometry of the work plane (cross section) under the geometry node.

At this point it should also be noted that in total five work planes were prepared as seen in Fig. 4.1. Of these two work planes are for the extended flow field on either sides of the matrix with slightly different cross sections from that of the channel to account for symmetry with adjacent channels. The remaining three serves to divide the channel and allows us to mesh these separately. A full view of the channel after extrusion with the extended flows (in green) on both sides of the channel are given as a reference below (Figure 4.2).

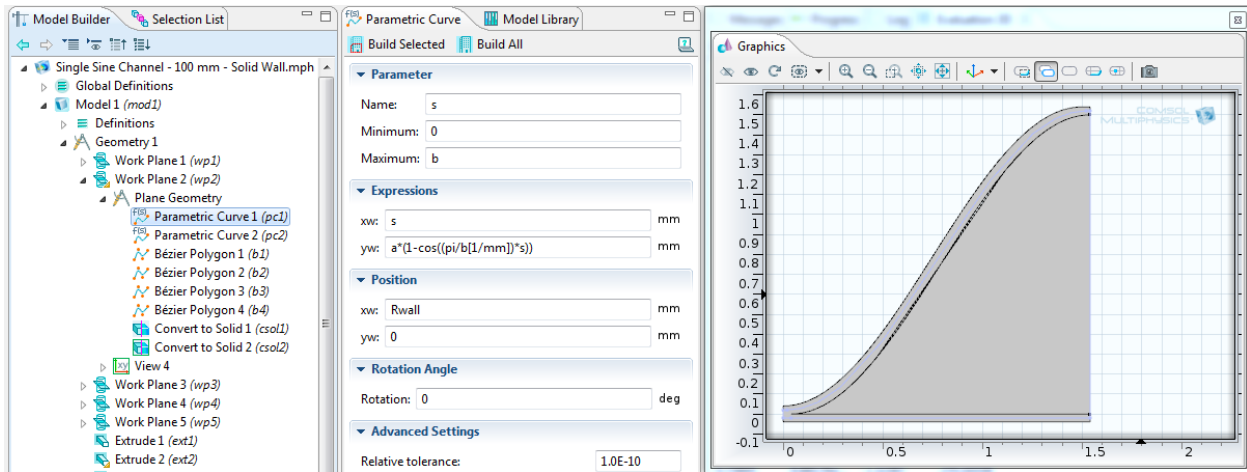


Figure 4.1 Geometry sequence together with parametric curve settings and sine geometry.

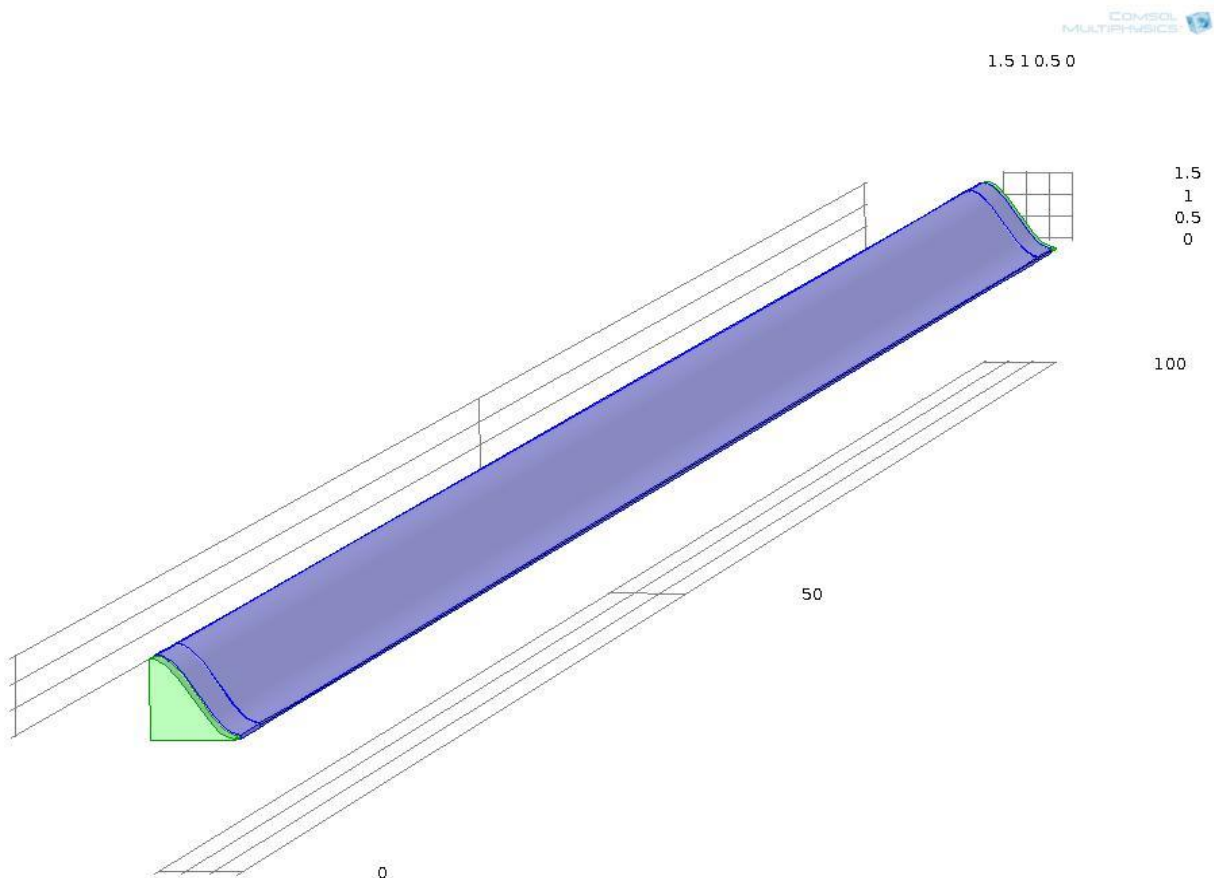


Figure 4.2 Three-dimensional representation of the sine channel

4.3 Velocity Problem

Our first step in this analysis is to establish how the flow geometry will express itself in the sine shaped channel of Figures 4.1 and 4.2. We've already established the governing equations, boundary conditions and initial conditions in equations (3.8-3.13), and hinted to the fact that these equations are in fact perfectly represented by the predefined single-phase laminar flow physics in *COMSOL Multiphysics*. Aside from setting up the physics using no-slip conditions, symmetry, and controlling the pressure and viscous stress on the appropriate boundaries, as defined by the geometry, the only unknown is the normal inflow velocity.

As noted before this velocity is defined as the face velocity in front of the wheel rather than as a uniform velocity at the inlet and is implemented by extending the flow field. The reasoning behind this ties to the heat transfer part of the analysis and comes as a consequence of a non-zero uniform velocity at the inlet. If the no-slip condition is violated at the inlet then automatically we will experience non-zero heat fluxes all over the inlet boundaries. As the neighboring boundaries of the matrix are thermally insulated the result would be heat flux discontinuities which are impossible to resolve. In addition as the initial temperature will always differ from the previous cycle (and as the switch from one of the air streams to the next is modeled as instantaneous) there will always exist an infinitely steep temperature gradient at the moment of transition. This cannot be resolved and will inevitably lead to ripples downstream. If we extend the flow field however and have a sufficiently fine mesh then the impact of these ripples will be minimized. Barring the strict numerical considerations the extended flow field also provides a more physically correct flow geometry as the air stream will be slowed down in front of the matrix frontal area as it is forced inside the channel. As such the additional computational requirement associated with simulating the flow upstream of the channel is deemed to be more than offset by both the numerical and physical considerations.

To construct the normal inflow velocity from our model parameters we begin by using moist air theory (see Appendix A) to find the correct mixture density from the temperature and relative humidity of the air stream feeding the matrix. When activating moist air as the fluid type in the *Heat Transfer in Fluids* interface it computes the thermodynamic properties of the air stream according to a given concentration field or an input quantity such as the mass fraction of water vapor. At the same time predefined functions which computes the saturated pressure for a given temperature, and either the moisture content or the molar water vapor concentration from the relative humidity, temperature and absolute pressure, becomes available. For now we limit ourselves to use the function which gives the saturated pressure to find the mixture density from the preliminary and mixture definitions as provided in Appendix A on moist air theory. The resulting set of relations leading to the mixture density is given in Table

4.2 below where the subscript s and e represents the supply and exhaust air streams, respectively.

Table 4.2 Flow geometry input variables

Name	Expression	Unit	Description
Xv_s	phi_supply*ht_f.fluid1.fpsat(T_supply)/1[atm]		Molar fraction of water vapor
Xa_s	1-Xv_s		Molar fraction of dry air
M_s	Xv_s*mat2.def.Mn+Xa_s*mat1.def.Mn	kg/mol	Mixture molecular weight
rho_s	((1[atm])*M_s)/(R_const*T_supply)	kg/m ³	Mixture supply density
u_face_s	2*m_supply/(rho_s*A_frontal)	m/s	Supply face velocity
Xv_e	phi_exhaust*ht_f.fluid1.fpsat(T_exhaust)/1[atm]		Molar fraction of water vapor
Xa_e	1-Xv_e		Molar fraction of dry air
M_e	Xv_e*mat2.def.Mn+Xa_e*mat1.def.Mn	kg/mol	Mixture molecular weight
rho_e	((1[atm])*M_e)/(R_const*T_exhaust)	kg/m ³	Mixture exhaust density
u_face_e	2*m_exhaust/(rho_e*A_frontal)	m/s	Exhaust face velocity
porosity	intop2(1)/intop3(1)		Wheel porosity
u_avg_s	u_face_s/porosity	m/s	Supply average velocity
u_avg_e	u_face_e/porosity	m/s	Exhaust average velocity

With the mixture density established as a function of the operating conditions we may apply a mass conservation statement on the flow just upstream of the channel. Assuming that the wheel is divided into equal sections for the supply and exhaust air streams the mass flow rate is given as,

$$\dot{m} = \frac{1}{2} \rho_m w_{face} A_{fr} \quad (4.1)$$

where ρ_m is the mixture density, A_{fr} is the wheel frontal area, and w_{face} is the face velocity.

Now simply solving for the face velocity as in the table giving the flow geometry input variables (Table 4.2) we have all the prerequisites needed to run an analysis on the flow geometry with a suitable numerical solver. As we will need to analyze the flow geometry to make sense of the subsequent sections on heat transfer we will skip ahead of the space discretization procedure for now and give the velocity profile at a cross section of the channel where the flow is considered to be fully developed (Figure 4.3). Additionally the z – dependent velocity profile in the hydrodynamic entrance region (Figure 4.4) at some arbitrarily chosen location (here $z = 0.25 \text{ mm}$) is also given as an illustration.

We observe that the maximum velocity occurs away from the centroid on the axis of symmetry in the contour plot giving the fully developed flow geometry (Figure 4.3) as was expected for the sine channel. As such no general statement can be made as for the location of w_{max} for the fully developed velocity profile and it has to be determined numerically. The z -dependent velocity profile in the hydrodynamic entrance region (Figure 4.4) shows clearly that as the velocity boundary layers grows there will exist local maxima because of the compressed corners together with an inviscid core as expected.

4.4 Conjugated Heat Transfer Problem

The conjugated problem as described in the mathematical model in the previous chapter contained a cascade of different concerns that needs to be dealt with in order to ready the formulation for analysis. First of all we require that the temperature and heat fluxes be continuous everywhere. In other words we need the boundary conditions of equations (3.11) and (3.12) to be appropriately imposed in such a way that the temperature fields and fluxes between the solid matrix and air stream are continuous.

Aside from how the different physics interfaces are coupled together we also need to implement the thermal boundary condition correctly. As we'll see not only are there uncertainties regarding the actual values of the peripheral averaged Nusselt numbers but from our discussion on thermal boundary conditions we remember that in a three-dimensional formulation we have to account for how it varies locally around the perimeter as well.

In defining the most appropriate thermal boundary condition, which we identified to be the (H1) boundary flux condition, we also introduced the concept of a bulk fluid mean temperature T_b . As we'll need that quantity along with the wall temperature T_{wall} to relate the convective conductance (or Nusselt number) to the heat flux we need to compute it from the flow geometry and local temperatures using the definition as set forth by equation (3.22) at every cross section along the axial direction.

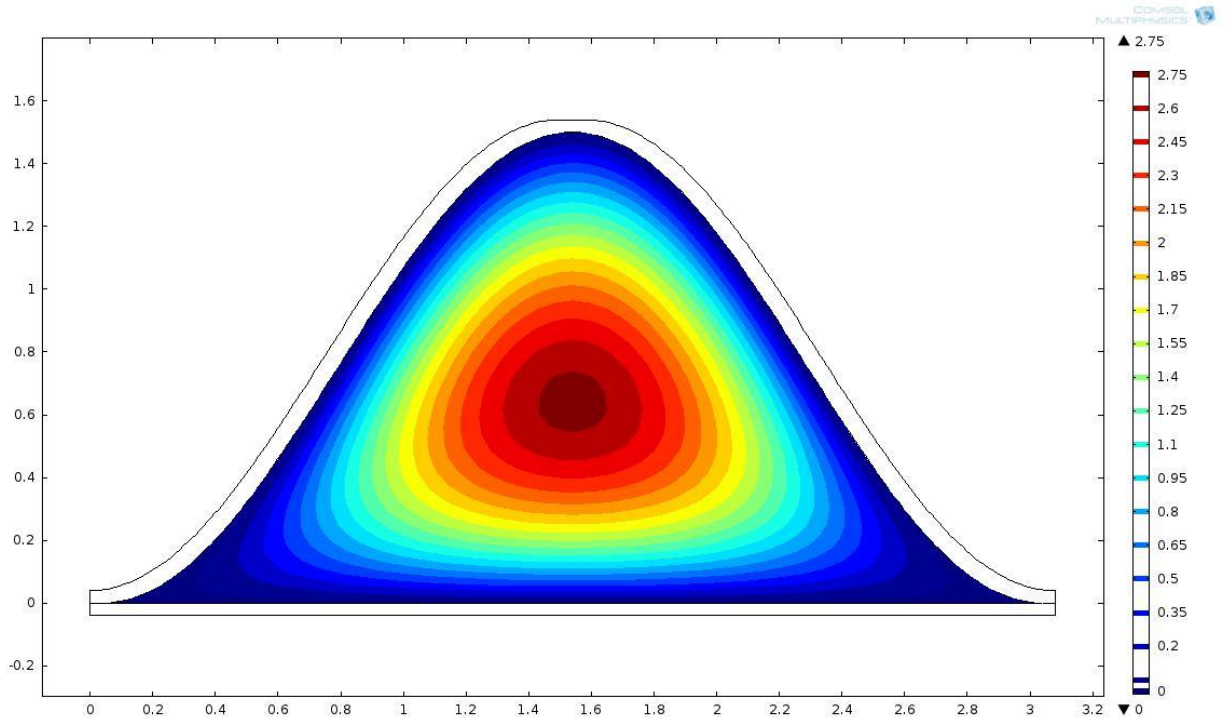


Figure 4.3 Contour plot of the fully developed velocity profile

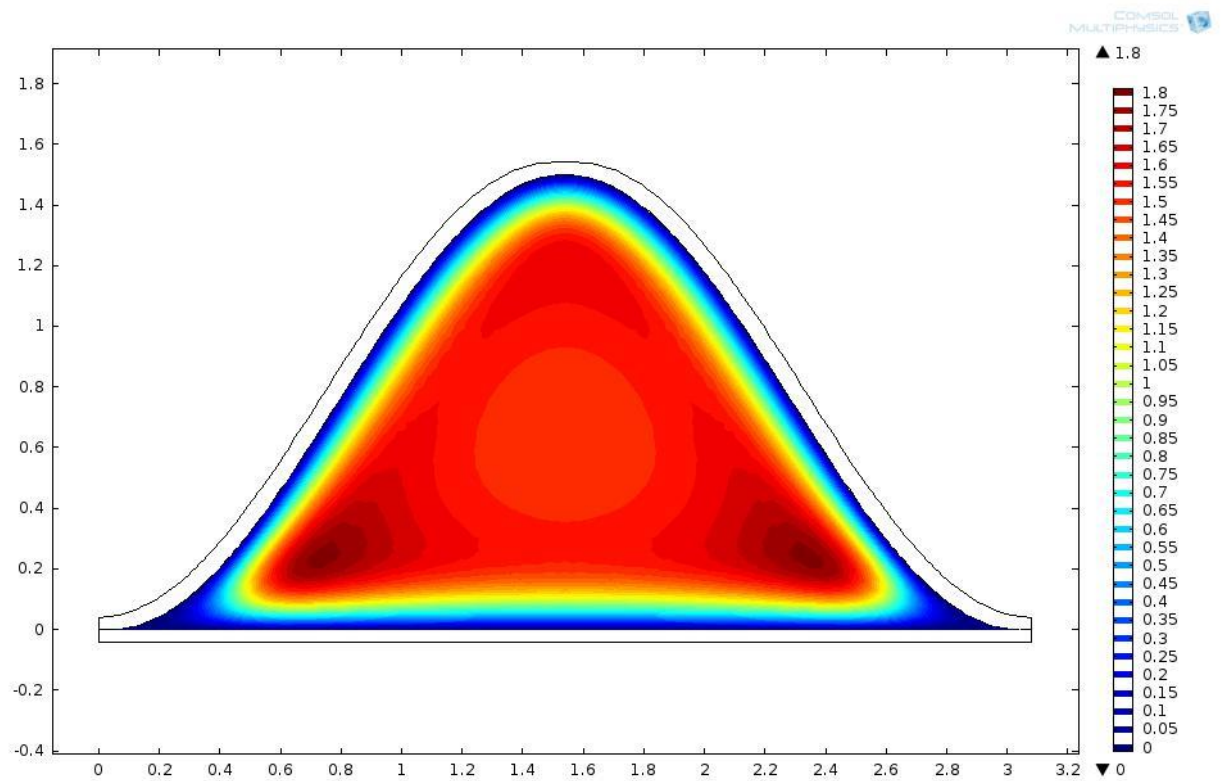


Figure 4.4 Contour plot of the developing velocity profile

4.4.1 Averaged Peripheral Nusselt Number

The fully developed laminar flow problem has been analyzed extensively for a range of duct geometries, including the sine geometry. As a result analytical correlations in closed-form equations have been developed and verified by many researchers for flow friction and heat transfer in a single channel. The hydraulic diameter and the averaged peripheral Nusselt number for a sine channel are available in terms of the ratio of the sine height to the sine length $\alpha^* = 2a/2b$ (c.f. Figure 3.1) as follows (Shah et al., 2003). For $0 \leq \alpha^* \leq 2$:

$$\frac{D_h}{2b} = (1.0542 - 0.4670\alpha^* - 0.1180\alpha^{*2} + 0.1794\alpha^{*3} - 0.0436\alpha^{*4})\alpha^* \quad (4.2)$$

$$Nu_{H1} = 1.9030(1 + 0.4556\alpha^* + 1.2111\alpha^{*2} - 1.6805\alpha^{*3} + 0.7724\alpha^{*4} - 0.1228\alpha^{*5}) \quad (4.3)$$

$$f \cdot Re = 9.5687(1 + 0.0772\alpha^* + 0.8619\alpha^{*2} - 0.8314\alpha^{*3} + 0.2907\alpha^{*4} - 0.0338\alpha^{*5}) \quad (4.4)$$

These relations are defined along with the modeling parameters (not shown in Table 4.1) and will automatically update according to the geometrical parameters. For the present case of $\alpha^* = 0.5$ the resulting geometrical, flow and heat transfer characteristics are $D_h = 1.2164 \text{ mm}$, $f \cdot Re = 11.170$, and $Nu_{H1} = 2.5975$, respectively.

Having the fully developed values we move on to find suitable Nusselt numbers for the simultaneously developing flow in the entrance region of the channel. Unfortunately no investigations has been (at least not successfully) conducted for the sine geometry for the simultaneously developing flow part, and as such no reliable data or empirical correlations is available for easy access to the author's knowledge. Our only option if we want to capture the increased heat transfer in this region is to turn to other similar geometries where data is available or, lacking that, to correlations available for developed flow and developing temperature profiles.

Simonson and Besant (1997) used data available in tabular form for the equilateral triangle duct geometry as presented in Shah and London (1978). These peripheral averaged Nusselt numbers were obtained using a finite difference method in which the effect of the transverse velocity components u and v , as well as the axial momentum and thermal diffusions, $\mu(\partial^2 w / \partial^2 z)$ and $k(\partial^2 w / \partial^2 z)$, respectively, were neglected. The resulting values are only valid for (and tabulated) in the region $1/200 \leq z^* \leq 1/10$ and are presented in Figure 4.5 along with the fully developed value for the sine geometry and a correlation for the Nusselt number in the case of developed flow (which we'll come back to later). In *COMSOL Multiphysics* this was achieved by using an interpolation function which allows us to use the tabulated values

directly and to apply a function to interpolate between the given values. The dimensional group governing the transition from the developing to the fully developed temperature profile is given as $z^* = z / (D_h \text{Re}_{D_h} \text{Pr})$ and the results are plotted against the square root of this value.

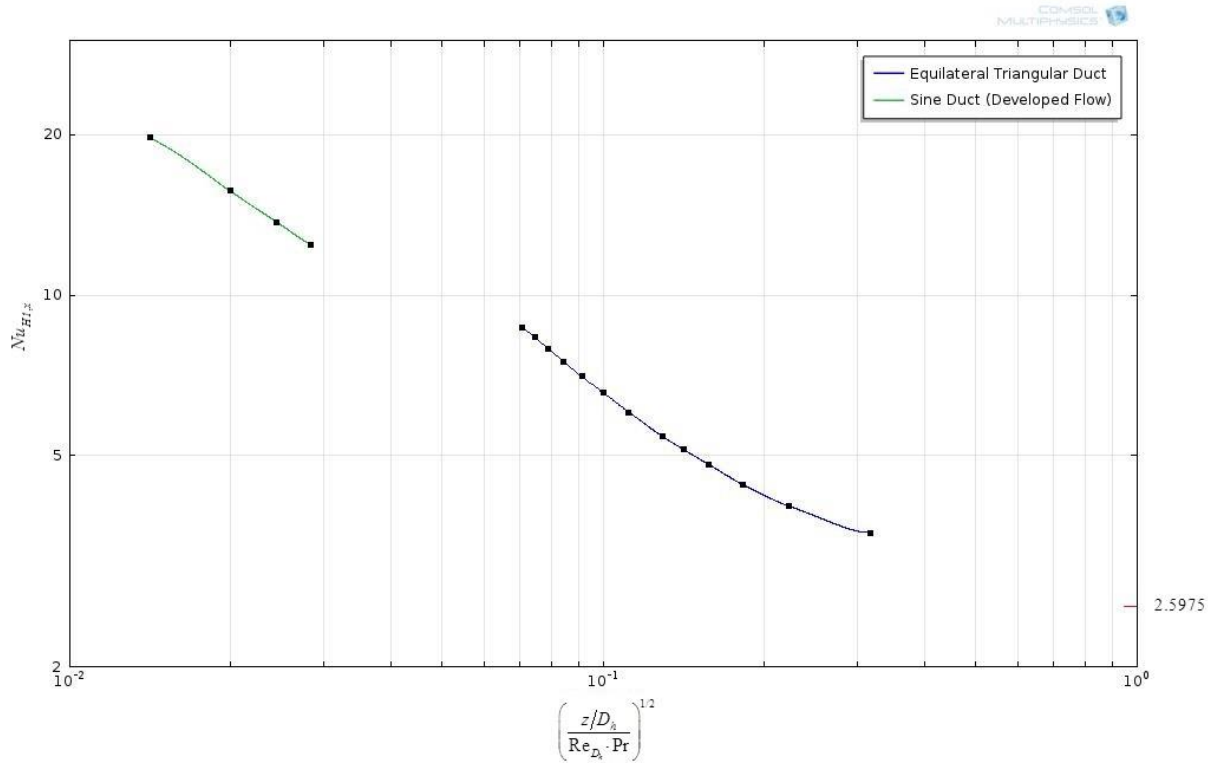


Figure 4.5 Heat transfer in the entrance region of a sine geometry with (HI) boundary condition

Now the fully developed value for an equilateral triangle duct with straight edges can be found in any book on convection heat transfer (c.f.(Shah and London, 1978)) to be $Nu_{H1,fd} = 3.111$ for the (HI) boundary condition while the value obtained at $z^* = 1/10$ using the scheme above were $Nu_{H1,z=1/10} = 3.58$. Clearly there is a discrepancy between these values that are unknown to us and to bridge the gap we need to know the thermal entrance length for which the Nusselt number approaches the fully developed value. Unfortunately no general formula is available to predict this thermal entrance length and even its definition as being the duct length required to achieve a value of local Nu_x equal to $1.05 Nu_{fd}$ for the fully developed flow are somewhat arbitrarily defined (Shah & London, 1978).

In addition we incidentally lack information on what happens as we're approaching the channel inlet and the best option seems to concede to using an correlation for the developed flow and developing temperature profile as sketched in Figure 4.5. The correlation is the result

of an regression analysis (Shah et al., 2003), and are given in terms of the product of the fanning friction factor and Reynolds number as provided through equation (4.4) and the dimensionless group as defined above:

$$Nu_{H1,z} = 0.517(f \cdot Re)^{1/3} (z^*)^{-1/3} \quad (4.5)$$

The above correlation are valid for both circular and noncircular ducts and are recommended for $z^* < 0.001$. Aside from leaving us with some blind spots as seen in Figure 4.5 it is important to recognize that if the velocity profile are already developed at the channel inlet the fluid velocity, velocity gradients, and temperature gradients near the wall will be lower than in the case of simultaneously developing flow. The higher the velocities near the wall the more thermal energy will be convected in the flow direction, and heat transfer in the thermal entrance region will therefore be higher in the case of developing velocity profiles.

Rather than settling with the above correlation then it may instead be prudent to return to some proper scaling analysis to find at least the correct scale for the thermal entrance length and deduce something about the nature of the profile of the developing Nusselt numbers. As a full scaling analysis is out of the scope of the present paper only the conclusions of an scaling analysis as performed by Bejan (2004) will be presented here and only in the case of $Pr \ll 1$ (the procedure is different but the conclusions the same in fluids like water and oils for which $Pr \gg 1$). If $Pr \ll 1$ then the thermal boundary layer δ_T develops faster than the velocity boundary layer δ and the following relation applies (Bejan, 2004),

$$\delta_T(z) \sim z Pr^{-1/2} Re_z^{1/2} \quad (4.6)$$

Now at the end of the thermal development $z \sim Z_T$ and $\delta_T \sim D_h$ so that,

$$Z_T Pr^{-1/2} Re_{Z_T}^{-1/2} \sim D_h \quad (4.7)$$

or

$$\left(\frac{Z_T / D_h}{Re_{D_h} Pr} \right)^{1/2} \sim 1 \quad (4.8)$$

This is a well-known result listed in much of the literature other than Bejan (2004) as,

$$\frac{Z_T / D_h}{Re_{D_h} Pr} \sim 0.1 \quad (4.9)$$

In view of the apparent discrepancy between these formulations Bejan (2004) makes the case that eq. (4.8) is the correct way of writing $\delta_T \sim D_h$. Squaring any proportionality in which the coefficient is $O(1)$ but numerically less than 1 Bejan (2004) argues, leads to a proportionality of type (4.9) where the coefficient is no longer $O(1)$. In conclusion then, the correct scaling for the transition from the developing to the thermally developed temperature profile is $\delta_T \sim D_h$, which means that the proper dimensionless group governing the transition is $\left[(Z_T/D_h) / (\text{Re}_{D_h} \text{Pr}) \right]^{1/2}$. The reason that this group (and its counterpart that describes the transition from the developing to the fully developed velocity profile) governs transition phenomena Bejan (2004) discusses is that they become of order 1 during transition. Moreover they become of order 1 because they represent the competition between the correct scales, which, after all, make the concept of transition meaningful (Bejan, 2004).

Applying the correct scale to the local peripheral average Nusselt numbers in the thermally developing section ($z \ll Z_T$) then gives,

$$Nu_z = \frac{hD_h}{k} \sim \frac{q''}{\Delta T} \frac{D_h}{k} \sim \frac{D_h}{\delta_T} \sim \left(\frac{z/D_h}{\text{Re}_{D_h} \text{Pr}} \right)^{-1/2} \quad (4.10)$$

Since the δ_T scale is $z \text{Pr}^{-1/2} \text{Re}_z^{-1/2}$ over the entire Pr range as alluded to before it follows that the Nusselt number scale of eq. (4.10) should be valid for all values of Pr (Bejan, 2004).

Returning now to the presented Nusselt numbers of Figure 4.4 it becomes obvious that when using the correct scale the developing Nusselt numbers should approach the fully developed value as the square root of our dimensionless group z^* becomes of $O(1)$. Clearly the simultaneously developing Nusselt numbers of the equilateral triangle duct does not approach the fully developed value of the sine duct but rather that of the fully developed value of the equilateral triangle duct. To rectify this discrepancy it is therefore proposed to modify the known values of the equilateral triangle duct by the factor $Nu_{fd,sine} / Nu_{fd,triangle}$ such that,

$$Nu_{z,sine} = \frac{Nu_{fd,sine}}{Nu_{fd,triangle}} \cdot Nu_{z,triangle} \quad (4.11)$$

On the other end of the domain of known Nusselt numbers we observe that the presented Nusselt numbers resulting from the correlation of eq. (4.5) seems to conform to the scaling law presented in eq. (4.10). This is indeed the case as in general, the results as cataloged in Shah and London (1978) show that in the entrance region ($z^{*1/2} \ll 1$), the Nusselt number obeys a relationship of the type (Bejan, 2004),

$$Nu_z = (constant) \left(\frac{z/D_h}{Re_{D_h} Pr} \right)^{-1/2} \quad (4.12)$$

where $(constant) = O(1)$. This proves the validity of the scaling law (4.10) and if we can find this constant for the simultaneously developing flow for the sine geometry we may complete the log-log presentation of Figure 4.5 as the scaling law has to exist in the form of lines of slope -1 .

Consider now the known Nusselt numbers of the modified sine duct as discussed above. Taking the difference between two of these at locations z_a and z_b ($z_a, z_b \ll Z_T$), and assuming that the Nusselt numbers obey the scaling law we have,

$$Nu_{z,a} - Nu_{z,b} = (constant) \left[\left(\frac{z_a/D_h}{Re_{D_h} Pr} \right)^{-1/2} - \left(\frac{z_b/D_h}{Re_{D_h} Pr} \right)^{-1/2} \right] \quad (4.13)$$

Now simply solving for the unknown constant, we get,

$$(constant) = (Nu_{z,a} - Nu_{z,b}) / \left[\left(\frac{z_a/D_h}{Re_{D_h} Pr} \right)^{-1/2} - \left(\frac{z_b/D_h}{Re_{D_h} Pr} \right)^{-1/2} \right] \quad (4.14)$$

and the log-log presentation may be completed using the Nusselt numbers that follows from eq. (4.12).

The resulting values are presented in Figure 4.6 along with the values of the equilateral triangle and the correlation of eq. (4.5) for comparison. As no successful investigation has been conducted on the simultaneously developing flow for the sine geometry it's difficult to assess the accuracy of these proposed Nusselt numbers, and the constant is if anything mildly speculative as it's only as good as the values of the modified sine duct Nusselt numbers derived from the equilateral triangular duct Nusselt numbers. In spite of this the presented values are following the scaling law (4.12) and therefore the general trend should be correct even if the Nusselt numbers should prove not to be accurate.

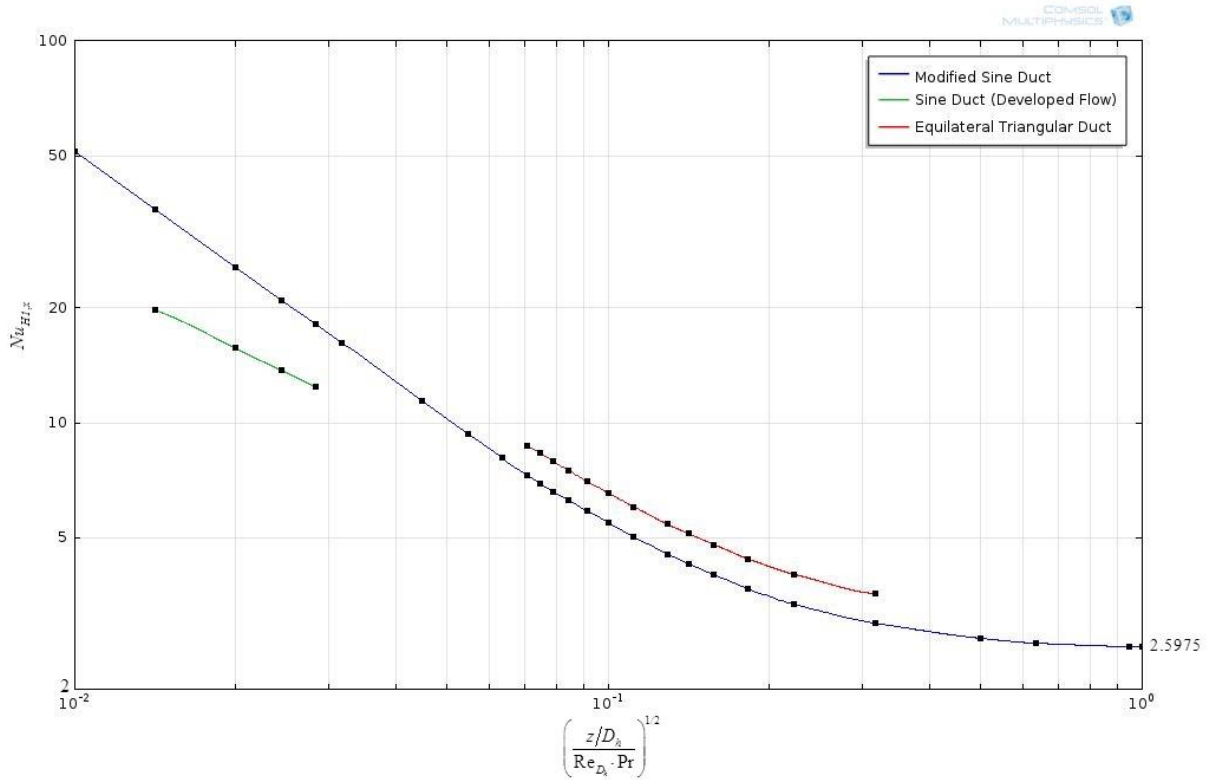


Figure 4.6 Heat transfer in the entrance region of a sine geometry with (HI) boundary condition

Having already defined the molar fractions of water vapor and dry air, the mixture density, and the average velocity of the air stream in the channel we continue using the moist air theory of Appendix A to define the rest of the needed thermophysical and transport properties of humid air. The resulting set of relations leading to the mixture Peclet number is given in Table 4.3 below where the subscript s and e represents the supply and exhaust air streams, respectively.

The target dimensionless group, z^* , can then be calculated according to the current distance z along the channel. In addition the average thermal conductivity of the mixture has been defined as the average of the thermal conductivities of the supply and exhaust air streams.

Table 4.3 Heat transfer input variables

Name	Expression	Unit	Description
r_Mnav	mat1.def.Mn/mat2.def.Mn		Ratio of molar mass of dry air to molar mass of water vapor
r_Mnva	mat2.def.Mn/mat1.def.Mn		Ratio of molar mass of water vapor to molar mass of dry air
r_mu_av_s	mat1.def.eta(T_supply[1/K])/mat2.def.eta(T_supply[1/K])		Ratio of air dynamic viscosity to water vapor dynamic viscosity
r_mu_va_s	mat2.def.eta(T_supply[1/K])/mat1.def.eta(T_supply[1/K])		Ratio of water vapor dynamic viscosity to air dynamic viscosity
phi_av_s	$(\sqrt{2}/4)^2(1+r_Mnav)^{-1/2}(1+r_mu_av_s^{1/2}r_Mnva^{1/4})^2$		Interaction parameter
phi_va_s	$(\sqrt{2}/4)^2(1+r_Mnva)^{-1/2}(1+r_mu_va_s^{1/2}r_Mnav^{1/4})^2$		Interaction parameter
Cpm_s	$(mat1.def.Mn/M_s)*Xa_s*mat1.def.Cp(T_supply[1/K])/J/kg/K+(mat2...$	J/(kg-K)	Mixture supply specific heat capacity
km_s	$(Xa_s*mat1.def.k(T_supply[1/K])/W/m/K)/(Xa_s+Xv_s*phi_av_s)+(Xv...$	W/(m-K)	Mixture supply thermal conductivity
Pe_s	$u_avg_s*D_hydraulic/(km_s/(rho_s*Cpm_s))$		Supply Peclet number
z_star_s	$z/(D_hydraulic*Pe_s)$		Dimensionless group
Cpm_e	$(mat1.def.Mn/M_e)*Xa_e*mat1.def.Cp(T_exhaust[1/K])/J/kg/K+(ma...$	J/(kg-K)	Mixture exhaust specific heat capacity
r_mu_av_e	mat1.def.eta(T_exhaust[1/K])/mat2.def.eta(T_exhaust[1/K])		Ratio of air dynamic viscosity to water vapor dynamic viscosity
r_mu_va_e	mat2.def.eta(T_exhaust[1/K])/mat1.def.eta(T_exhaust[1/K])		Ratio of water vapor dynamic viscosity to air dynamic viscosity
phi_av_e	$(\sqrt{2}/4)^2(1+r_Mnav)^{-1/2}(1+r_mu_av_e^{1/2}r_Mnva^{1/4})^2$		Interaction parameter
phi_va_e	$(\sqrt{2}/4)^2(1+r_Mnva)^{-1/2}(1+r_mu_va_e^{1/2}r_Mnav^{1/4})^2$		Interaction parameter
km_e	$(Xa_s*mat1.def.k(T_exhaust[1/K])/W/m/K)/(Xa_s+Xv_s*phi_av_s)+(X...$	W/(m-K)	Mixture exhaust thermal conductivity

4.4.2 Local Peripheral Nusselt Number

As was discussed in the section on the thermal boundary condition in the chapter describing the mathematical model, the near uniform wall temperature around the noncircular periphery of the channel dictates that the peripheral local heat flux in turn must be variable around the periphery. Since information about the distribution of the peripheral local heat flux around the periphery of the sine geometry is non-existent in the literature we again have to rely on information we can salvage from investigations conducted on other geometries and general observations on how the peripheral local heat flux must behave to accommodate the flow geometry.

There are various analytical, semi-analytical and numerical methods available for the solution of the relevant momentum and energy equations, but most of these are only concerned with laminar fully developed flows and with the peripheral averaged Nusselt number (c.f.(Sherony & Solbrig, 1970)). Now the analytical treatments are generally only applicable to simpler geometries so that no closed-form solution are available and as such we expect any investigation to be performed using either semi-analytical or numerical techniques. We've already established that no such study is available for the sine geometry, let alone for the developing region, and moreover note that any such investigation would have to provide a function for the local peripheral Nusselt number that takes into account the flow geometry to be directly applicable in the present analysis.

Still the work of Ray and Misra (2010), which provides a detailed description of the local peripheral Nusselt number for the rectangular and equilateral triangular geometries with

varying radius of curvature at the corners, is interesting. Their investigation revolved around a semi-analytical approach in which the least-square method were employed on harmonic series and showed excellent agreement against previous studies when comparing the peripheral averaged Nusselt number. What makes it interesting however is that it confirms that the heat flux will indeed drop to zero in the case of a sharp corner for both the rectangular and equilateral triangular geometries, and that the heat transfer coefficient is at a maximum at the straight portions of the channel. As such the influence of the flow geometry is demonstrated in that sharp corners where adjacent walls converge acts as a heat (or cold) pocket because of the lower axial velocity while the straight-portions with less restricted flow transfer heat more effectively. The coupling between the flow geometry and the temperature is in Ray and Misra (2010) made clear by the fact the known coefficients of the harmonic series solution of the velocity problem is used as part of the series solution of the temperature problem.

Returning now to the fully developed velocity profile of Figure 4.3 we may make some general observations about the nature of the local peripheral Nusselt number around the periphery of the sine geometry. As observed for the geometries analyzed in Ray and Misra (2010) the local heat flux (and Nusselt number) has to drop to exactly zero in the corner where the walls converge. The rate of change of the local heat flux approaching this singularity will moreover be dependent on the local area goodness factor (wall-to-wall distance) resulting from the curvature of the sine curve and the flat plane. Next there has to be local maxima on the axis of symmetry on the flat plane and somewhere on the sine curve where the resistance to flow is at a minimum. Finally the decrease in Nusselt number in the uppermost region must have a local minima on the axis of symmetry that again will depend on the local area goodness factor resulting from the radius of curvature around this point.

Based on these observations it is therefore proposed that the local peripheral Nusselt numbers will be a function of the rate of change of the velocity gradient from the maximum velocity on the axis of symmetry to the requirement of zero velocities on the walls. The rate of change is clearly observed in Figure 4.3 where consecutive layers of lines of constant velocity is dense approaching the expected local maxima, and more spaced towards the uppermost region and sharp corners where the local area goodness factor rapidly declines. As the averaged peripheral Nusselt number at any cross-section z along the axis is known we may write (c.f. eq. (3.15)),

$$Nu_z = \int_{\Gamma} Nu_{p,z} ds = Nu_z \int_{\Gamma} f(s) ds \quad (4.15)$$

assuming that the local peripheral Nusselt number can be expressed as the product of the averaged peripheral Nusselt number and some function $f(s)$ subject to,

$$\int_{\Gamma} f(s)ds = 1 \quad (4.16)$$

where p denotes the local peripheral value and $f(s)$ is defined as the peripheral local Nusselt number function.

To find this function we begin by making the observation that the rate of change of the velocity gradient from the maximum velocity on the axis of symmetry scales with the distance from the maximum velocity to the wall. This distance is simply given as,

$$d(x, y) = \left((x - x_{\max})^2 + (y - y_{\max})^2 \right)^{1/2} \quad (4.17)$$

where (x_{\max}, y_{\max}) is the location of the maximum velocity for the fully developed flow, and (x, y) are local wall coordinates. The coordinates for the maximum velocity can be found using a maximum operator defined on the domains of the air stream.

Using this distance we may define the minimum and maximum wall distances from the maximum velocity to the sharp corner and the global maxima (which may correspond to either the flat plane or some point on the parametric curve) as d_{\min} and d_{\max} , respectively, by way of a minimum and maximum operator defined on the wall boundaries facing the air stream. The peripheral local Nusselt number function can then be recast in terms of the distance d as,

$$\int_{\Gamma} f(s)ds = \alpha \int_{\Gamma} f(d)d\zeta = 1 \quad (4.18)$$

where $\alpha = 1 / \int_{\Gamma} f(d)d\zeta$ is an area correcting factor, ζ a dummy variable, and $f(d)$ is given as,

$$f(d) = \beta(d) \cdot \left(1 - \frac{d - d_{\min}}{d_{\max} - d_{\min}} \right) \quad (4.19)$$

where $\beta(d)$ is some function taking into account the local area goodness factor at location $d(x, y)$ on the wall.

The set of relations as defined above are given below (Figure 4.6) along with the boundaries on which these equations are valid. Here the local area goodness factor function is simply set to $\beta(d) = (d_{\max} - d) / d_{\max}$ too further shift the heat transfer away from the sharp corner. As seen the local peripheral Nusselt number on the neighboring boundaries facing adjacent air streams are also defined using the skew-symmetry boundary condition. This involves defining an alternative coordinate system in which the wall distance is subject to an

imaginary maximum velocity in the neighboring channels and may be achieved by mirroring the known values on the boundaries of the simulated air stream in an appropriate fashion to create reciprocal (skew) values on the boundaries facing the adjacent air streams. The subscripts s and e denotes the supply and exhaust air streams respectively, as before.

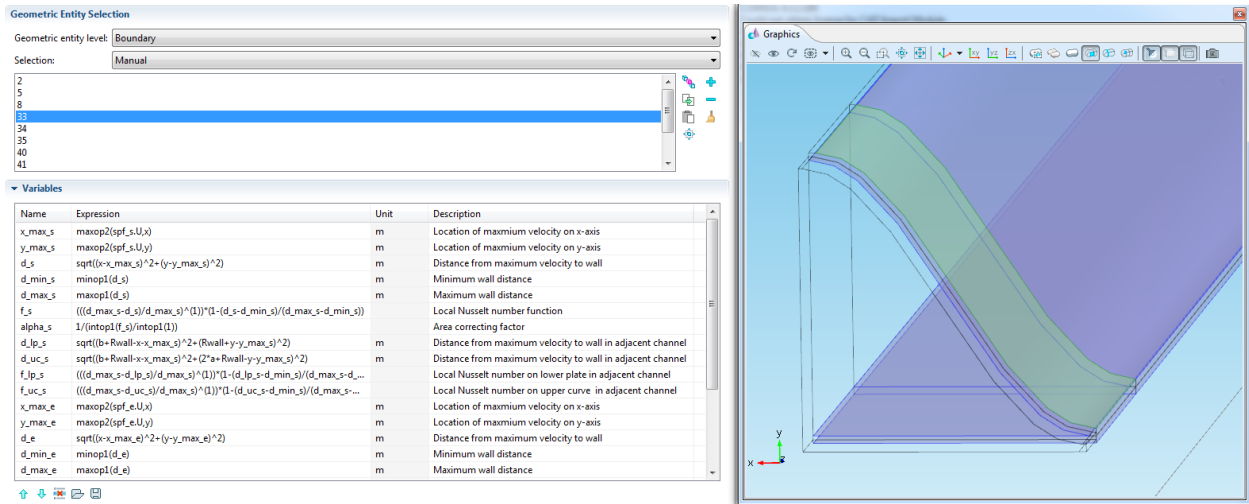


Figure 4.7 Local peripheral Nusselt number function with associated boundaries

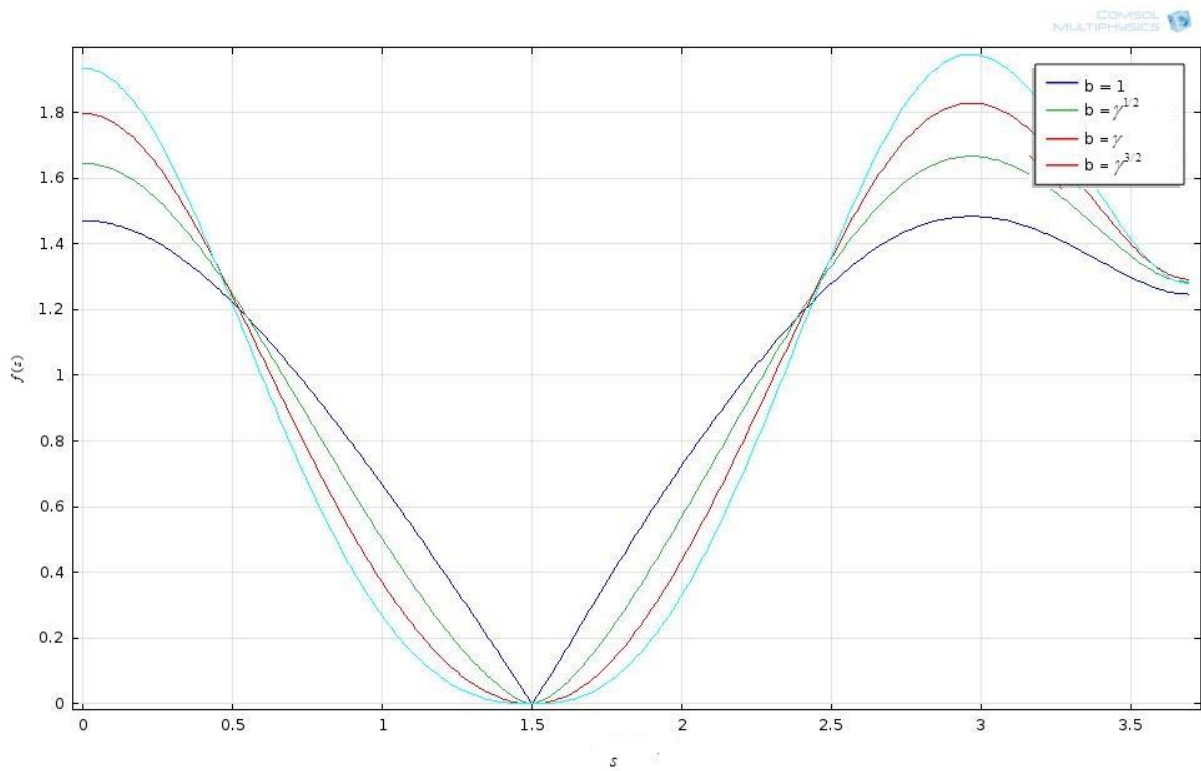


Figure 4.8 Local peripheral Nusselt number function as a function of s along the periphery

The resulting peripheral local Nusselt number function can now be plotted against the wall distance s along the periphery, starting from the axis of symmetry on the flat plane and ending on the axis of symmetry on the uppermost portion, for various functions $\beta(d)$ taking into account the local wall-to-wall distance (Figure 4.8).

Now all of these are in line with the general pattern we expect to see around the periphery as discussed in the preceding section, with $\beta = 1$ giving the unadulterated distance function and $\beta = \gamma^n$ where $\gamma = (d_{\max} - d)/d_{\max}$ giving consecutive shifts of more heat transfer taking place away from the point of singularity. The most reminiscent curve of the rectangular geometry in the case of the H1 boundary condition in Ray and Misra (2010) is $\beta = 1$ while for the equilateral triangular geometry it seems to shift towards something similar to $n > 0$. Considering that the wall-to-wall distance in the sharp corner of the sine geometry is even less than that of the equilateral triangle (which again is less than the rectangular geometry) we can with some confidence rule out the pure distance function but the exact value of n remains unknown. Indeed it may be that some other function $\beta(d)$ other than those considered here would be more suitable. In the present analysis we choose, somewhat arbitrarily, the coefficient to be $n = 1/2$.

The above analysis still has merit of course using the z – dependent velocity profile present in the hydrodynamic entrance region, but is complicated by the fact that the velocity profile is developing. Starting out as near uniform at the entrance the flow geometry will immediately adapt to the local area goodness factor of the compressed corners resulting in local increased velocities while the inviscid core remains unaffected (see Figure 4.4). As the velocity boundary layer around the periphery continues to grow these pockets of higher velocity will propagate towards the axis of symmetry along with a pocket of local increased velocity in the uppermost region that similarly is the result of a competition between the appropriate scales. Initially then we expect the peripheral local Nusselt numbers to be much more uniformly distributed around the periphery with local maxima starting closer to the singularity (where the heat flux is still zero) on both the sine and flat plane, together with a local maxima on the axis of symmetry in the uppermost region. Then as the velocity boundary layers develops these local maxima will start to approach the local maxima as seen in the fully developed peripheral local Nusselt number function of Figure 4.8 from both sides of the sine and on the flat plane.

Now to implement this in our mathematical model in *Comsol Multiphysics* we would begin with keeping track on all local maxima at every cross section along the flow axis and impose some function that would yield local maxima at the appropriate locations while at the same maintaining zero heat flux at the singularity. This is out of the scope (or timeframe) of the

present analysis and instead we are forced to assume the fully developed peripheral local Nusselt number function holds in the simultaneously developing region as well. Combining the averaged peripheral Nusselt number with the peripheral local Nusselt number function we can then plot the resulting Nusselt numbers directly on the wall boundaries facing the air stream along with the imposed skew-symmetry Nusselt numbers of the neighboring channels (Figure 4.9).

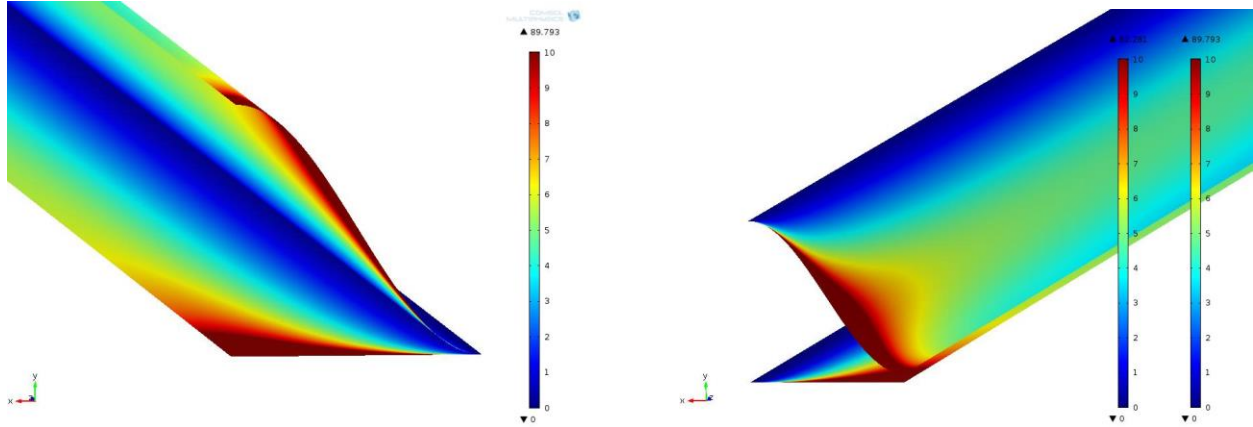


Figure 4.9 Local Peripheral Nusselt numbers in the entrance region for (a) the channel and for (b) the skew-symmetry boundaries (color range capped at $Nu \leq 10$ for illustration purposes)

4.4.3 Defining the Bulk Temperature

To complete the relationship between the heat flux q'' and the Nusselt number we finally require the wall-fluid temperature difference. As was discussed in the chapter on the thermal boundary condition we conventionally select $\Delta T = T_{wall} - T_b$ as the representative wall-fluid temperature difference since the fluid temperature varies over the channel cross section. The fluid bulk mean temperature T_b is not just any average; it is the mean temperature the definition of which is the first law for bulk flow (Bejan, 2004). Its definition was given as eq. (3.22) in the section on the thermal boundary condition in the previous chapter and is rewritten here as the following double integral over x and y .

$$T_b(z) = \frac{1}{A_c \cdot w_b} \iint w(x, y, z) \cdot T(x, y, z) dx dy \quad (4.20)$$

where A_c is the constant cross-sectional area and w_b the bulk velocity.

To evaluate this double integral in *Comsol Multiphysics* we can use two general projection coupling operators. How they work are not straight-forward and may arguably best be described by way of an shadowgraphy analogy. In such an analogy the model (or part of it) takes the role of the hands and are defined as the source in the operator settings. The wall in this analogy is another part of the model: the destination. This is where the shadow is formed. Just like shadow puppets then, the result of a projection is to reduce the dimension of the source by one. The projected quantities or image is formed by integrating an expression in the direction of light. This direction is specified by a map between the source and the destination.

Now consider first projecting from 3D to 2D by integrating over y (the x – direction would work equally well here) over a representative cross-section of the channel as in the upper-left corner of Figure 4.10 below. Here the red arrows represent the lines integrated over. The associated operator's settings contain fields for mathematical expressions where we can define the source map and the destination map. As there's no need to integrate over some curve the expressions will simply be linear functions of the coordinates, and starting with the destination map we simply enter z and x in the x and y expressions, respectively, to define the flow axis z and the x axis as the destination of the projection. Since we use the same plane in the source, the x and y expressions are z and x there as well. The z expression then defines the direction of integration, which in this case is the y axis, so we simply enter y .

The next step then is to use another projection operator to project the results of the first operator as described above from 2D to 1D by integrating over the remaining coordinate. Presented again at a representative cross-section of the channel we see the intended lines of integration as red arrows in the upper-right corner of Figure 4.10. As for the first projection operator this procedure takes place along the whole length of the flow axis, only this time we integrate over the boundary associated with the flat plane and not the entire flow domain. The destination map then is simply the z axis so we enter z in the x expression. Since we use the same line in the source, the x expression are z here as well. The y expression now defines the direction of integration so we simply enter the remaining coordinate x .

We can now use these projection operators (called *genproj1* and *genproj2* for the 3D to 2D and the 2D to 1D projection, respectively) in combination to evaluate the mean bulk temperature as defined in eq. (4.20) as follows.

$$T_b(z) = \frac{1}{A_c \cdot w_b} \iint w(x, y, z) \cdot T(x, y, z) dx dy = \frac{\text{genproj2}(\text{genproj1}(w \cdot T))}{\text{genproj2}(\text{genproj1}(w))} \quad (4.21)$$

where $A_c \cdot w_b = \iint w(x, y, z) dx dy = \text{genproj2}(\text{genproj1}(w))$ has been defined as a nested projection as well to ensure consistency.

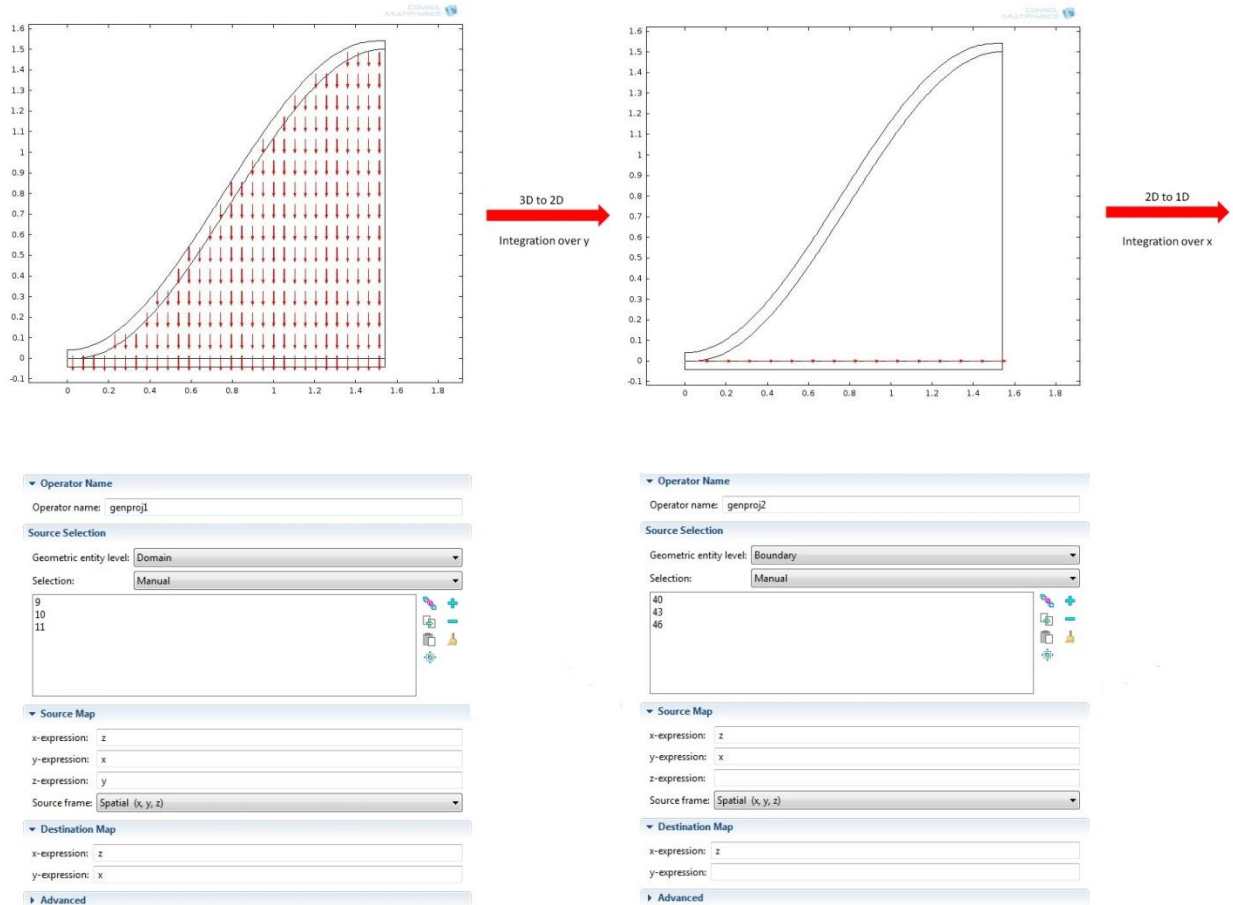


Figure 4.10 Conceptual drawing of the lines of integration with associated General Projection settings.

Now we could seemingly use the expression for the nested projection of eq. (4.21) directly in the heat flux defined on the heat flux boundaries but that would lead to a problem that is unnecessarily complex. Consider that with only one level of projection, the heat flux in every node on the heat flux boundaries connects to all nodes in a domain or on a boundary. With two levels, the same heat flux connects to one integral over all nodes in a domain or on a boundary, for each node in a domain or on a boundary. While the details of the assembly process are too involved to be presented here it is nevertheless clear that the vastly increased levels of complexity that results from nesting two projections and applying the result on a boundary will lead to an prohibitively long assembly time.

Instead it is proposed to define an edge ODE, mapping the nested projection to an edge variable T_b . This can be achieved by simply adding the Edge ODE and DAEs physics from the Mathematics module, which enables us to configure the following equation on any edge in the geometry.

$$e_a \frac{\partial^2 T_b}{\partial t^2} + d_a \frac{\partial T_b}{\partial t} = f \quad (4.22)$$

Now simply setting the coefficients e_a and d_a to zero as in the distributed ODE column of Figure 4.10 we can map the nested projection onto the edge variable T_b by simply subtracting the nested projection from the edge variable in the source term f . Then with the help of a general extrusion (which allows us to map an expression defined on a source to an expression evaluated on any destination as shown in the general extrusion column of Figure 4.11) defined on the same edges (marked in blue in the graphics of Figure 4.11) as the edge variable T_b , we may again apply the heat flux on the appropriate heat flux boundaries.

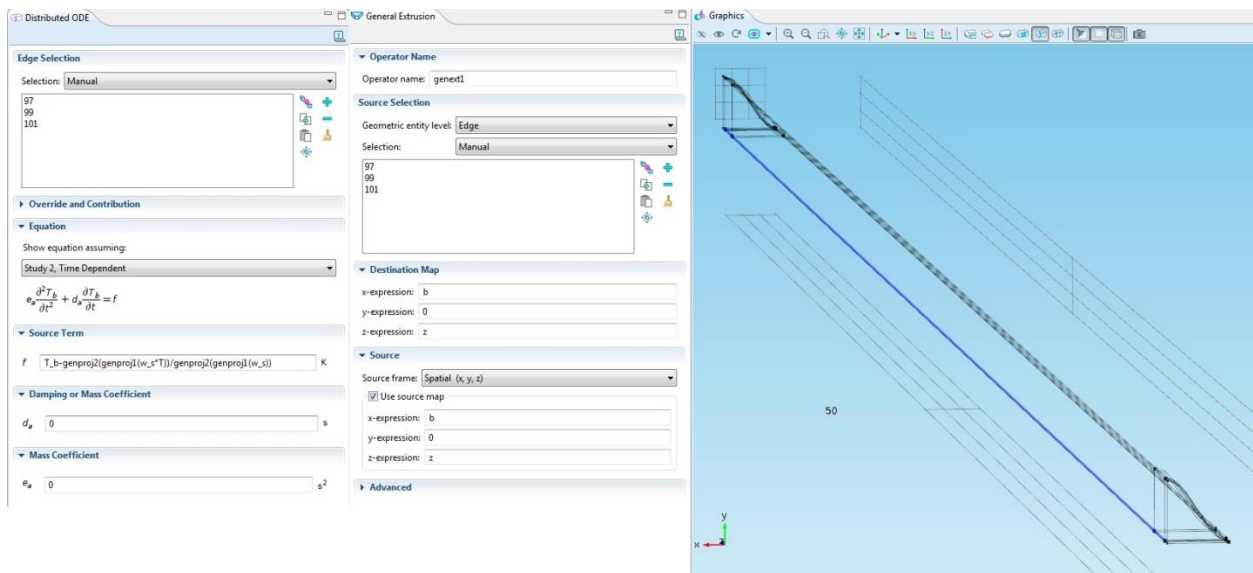


Figure 4.11 Edge ODE and DAEs and General Extrusion Coupling settings with associated edges

In the assembly process the difference now is that while the nested projection as stated needed to be performed once for every node on the heat flux boundaries, the nested projection mapped on the edge variable T_b only needs to be performed once for every node on the selected edges.

4.4.4 Imposing the Thermal Boundary Conditions

The final step in completing the formulation of the conjugated heat transfer problem aside setting up the physics using symmetry (which gives the same equation as thermal insulation in this case), thermal insulation and designating the inlet temperature and outflow

on the appropriate boundaries (see Figure 4.12) is to couple together the matrix temperature and the air stream temperature using the appropriate thermal boundary conditions.

Now we do have some freedom in what physics interfaces we choose to use in order to implement the conjugated problem as defined by equations (3.11-3.17), but as we've already discussed the *Heat Transfer in Fluids* physics coupled together with either the *Heat Transfer in Solids* or the *Heat Transfer in Thin Shells* physics presents itself as most suitable to our application. Here we will use the former (*Heat Transfer in Solids*) as it has proven to be far easier to define the geometry, the thermal boundary conditions and the peripheral local Nusselt number function correctly using this interface. On the other hand the latter (*Heat Transfer in Thin Shells*) frees us of the need to define the mesh in the solid matrix and is more computationally efficient than its counterpart as it is tailored for these exact situations. Unfortunately there are issues concerning the geometry that leads to problems with the thermal boundary conditions and the peripheral local Nusselt number function that cannot be resolved without inducing some level of error, that may or may not be acceptable.

Moving on to the objective of coupling the physics together we begin by defining the heat fluxes that the matrix boundaries are subject too. The heat flux in the direction of the matrix on the wall-fluid interface are given combining the averaged peripheral Nusselt number, the peripheral local Nusselt number function and the wall-fluid temperature difference as,

$$q''(z, s) = f(s)Nu_{HI,z}(z^*)\frac{k}{D_h}(T_b(z) - T_{wall}) \quad (4.23)$$

where $f(s) = \alpha f(d)$.

The skew-symmetry heat fluxes are similarly defined on the outside boundaries only now the skew-symmetry functions $f_{lp}(s)$ and $f_{uc}(s)$, for the lower plate and upper curve, respectively, replaces the peripheral local Nusselt number function $f(s)$. These heat fluxes are implemented as shown in Figure 4.12 as *Heat Flux 1, 2 and 3*, respectively, by selecting the appropriate boundaries and using the native variables as defined previously together with the interpolation function $Nu_HI_z(z_star)$ giving the averaged peripheral Nusselt number.

Now in order to implement the requirement that the temperature and heat flux are both continuous as expressed by the boundary conditions of eq. (3.11) and (3.12) we simply designate the temperature of the air stream to be $T = T_{wall}$ (*Temperature 2* in Figure 4.12) on all shared boundaries. The heat flux across this common boundary will then everywhere be exactly what is must be in order for the equations and the remaining boundary conditions put forward to be fulfilled. To see why it has to be this way imagine that we were to manually specify both the temperature and the heat flux on the shared boundaries. Then either the temperature

condition or the heat flux condition would automatically override the other because if it didn't we would be over-constraining the system of equations. Moreover if we attempted to assign only a heat flux condition in lieu of the temperature condition we would violate the continuity equation and the air stream temperature immediately adjacent to the wall-fluid interface would not be constrained by the matrix temperature.

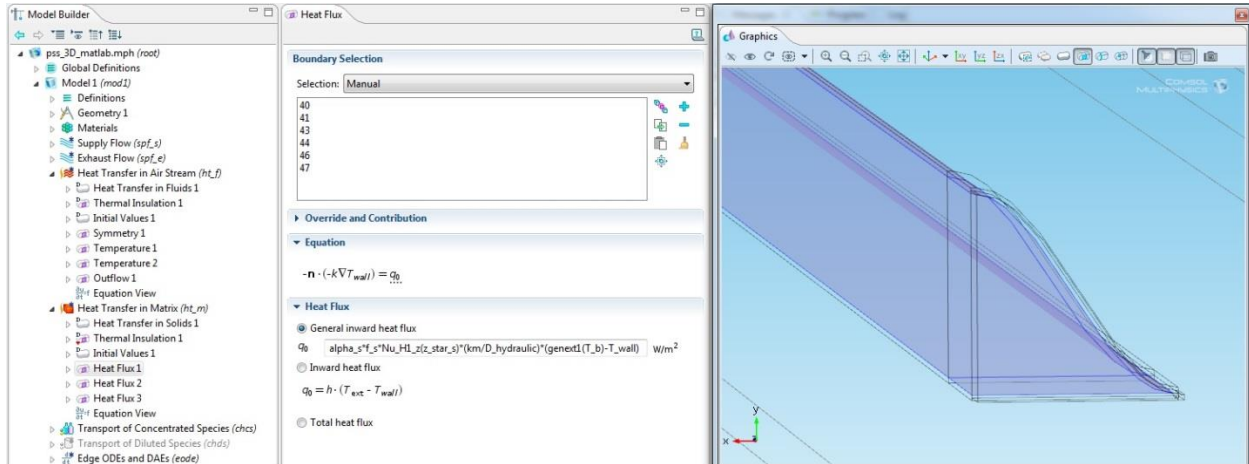


Figure 4.12 Heat flux settings with associated boundaries

4.5 Mass Conservation of Constituents in the Air Stream

The mass conservation of dry air and water vapor expressed in terms of either mass fractions or molar concentrations together with their associated boundary and initial conditions may be implemented using the *Transport of Concentrated Species* interface or the *Transport of Diluted Species* interface, respectively. Here we choose to use the formulation consisting of eqs. (3.25-3.27) corresponding to the Transport of Concentrated Species interface as it arguably is a more familiar way to write the concentration equation.

In any case we begin by again noting the similarities between the mass convection problem and the energy convection problem. If we divide the energy equation of (3.11) with ρC_p and compare it with the concentration equation of (3.25) we observe that the mass fraction pw_i occupies the place of the temperature, while the mass diffusivity D replaces the thermal diffusivity $\alpha = k/\rho C_p$. As such we can set up the physics in the same manner as the fluid temperature problem with symmetry, inlet mass fraction and outflow on the same boundaries. The only difference is that since we in the present analysis assume that the air stream does not exchange moisture with the matrix through neither sorption nor condensation

(which would lead to extra terms in the energy equation) the mass boundary condition reduces to simply a statement of no mass flux across the wall-fluid interface.

The dominating feature of the concentration profile is thus simply the inlet mass fraction together with some weak concentration gradients caused by the mass diffusivity. The inlet mass fraction can simply be found using moist air theory (Appendix A), and a feature in *COMSOL Multiphysics* even allows us to define it in terms of the molar concentration. As discussed earlier in regard to the saturated pressure a predefined function is also available to determine the molar concentration directly from the modeling parameters of temperature, relative humidity and absolute pressure, and so it makes sense to exercise this option.

The mass diffusivity D is as was alluded to in the beginning of this chapter dependent on the mixture temperature and pressure and can be evaluated using the value specified in the table as (Bejan, 2004),

$$D(T, p) \cong D(T_0, p_0) \left(\frac{T}{T_0} \right)^{1.75} \frac{p_0}{p} \quad (4.24)$$

where $T_0 = 298 \text{ K}$ and p_0 is atmospheric pressure.

Worth keeping in mind is that the mass diffusivity of a binary gaseous mixture does not depend on the concentration. Now as the diffusive term is expected to be almost negligible compared to the convective term in eq. (3.25), small changes in the value of the diffusivity coefficient is likely to have minimal impact on the results. As such it is prudent to simply assume that the mass diffusivity D is constant with little loss of accuracy.

4.6 Space Discretization

The final operation in completing the numerical model is to define the set points that replaces the continuity of the real space by a finite number of isolated points or elements in space. As was briefly discussed in defining the discretization process the grid properties, quality and mesh size is instrumental to the outcome of the simulation and its accuracy. As the mesh size decreases towards zero (leading to a model of infinite size) we move toward the exact solution for the equations we are solving. However, as we are limited by both finite computational resources and time, we have to rely on an approximation of the real solution. The goal then is to construct a mesh that allows for a simulation to be performed where the difference or error between the exact and the approximated solution is minimized such that it is below some accepted tolerance level.

Now given the huge array of possible ways to combine the different element types it becomes clear that we need some strategy when constructing the mesh. The first option would

normally be to just default to a physics-controlled mesh automatically available as a meshing sequence, but in the sine geometry considered in this paper it fails as a result of the complexity of the geometry. Instead the mesh has to be user-controlled, and while we will not concern ourselves with the exact procedure here a few remarks on how it may be done and potential concerns are appropriate.

As a result of the skewed aspect ratio $L/D_h \gg 1$ and thin wall it seems prudent to use some form of swept mesh so that the cross-sectional xy – plane mesh remains the same through the entire length of the channel. In an alternative scenario we could envisage to control all the boundaries around the periphery and use an unstructured tetrahedral mesh. Either way we would want to define the mesh at $z = 0, L$ using some sort of combination of a mapped mesh and a free triangular mesh on the appropriate boundaries. To further control the interaction between the meshes corresponding to the air stream and matrix we could also make use of an edge mesh around the periphery. In addition we should consider including a boundary layer mesh which are typically used for fluid flow problems to resolve the thin boundary layers along the no-slip boundaries.

Next to ensure that the grid stretching is continuous along the flow axis we need to assign some distribution to take into account the more abrupt gradients present in the entrance region. As we've already separated the channel into multiple regions one option is to assign a geometric distribution giving a dense mesh at the inlet that is progressively more spaced along the domain covering the entrance region. Then for the remainder of the channel where gradients is expected both to be of approximately the same magnitude and to have a major longitudinal component we can assign a fixed distribution giving equal spacing.

Completing these steps gives a mesh reminiscent of Figure 4.13 and Figure 4.14 where the xy – plane and entrance region together with a mesh sequence are displayed, respectively.

What's apparent in the sample meshes given (Figure 4.13) is that the decision of including or not including a dedicated boundary layer mesh around the periphery will result in two meshes that differ considerably with respect to element quality and total number of elements. To find how they compare then we need to take a look at the mesh statistics which gives a detailed report of the mesh elements. As we have the option to examine the meshed edges, boundaries and domains individually we select the boundary corresponding to the air stream at the channel opening for a simple analysis. The resulting set of statistics are given below in Figure 4.15.

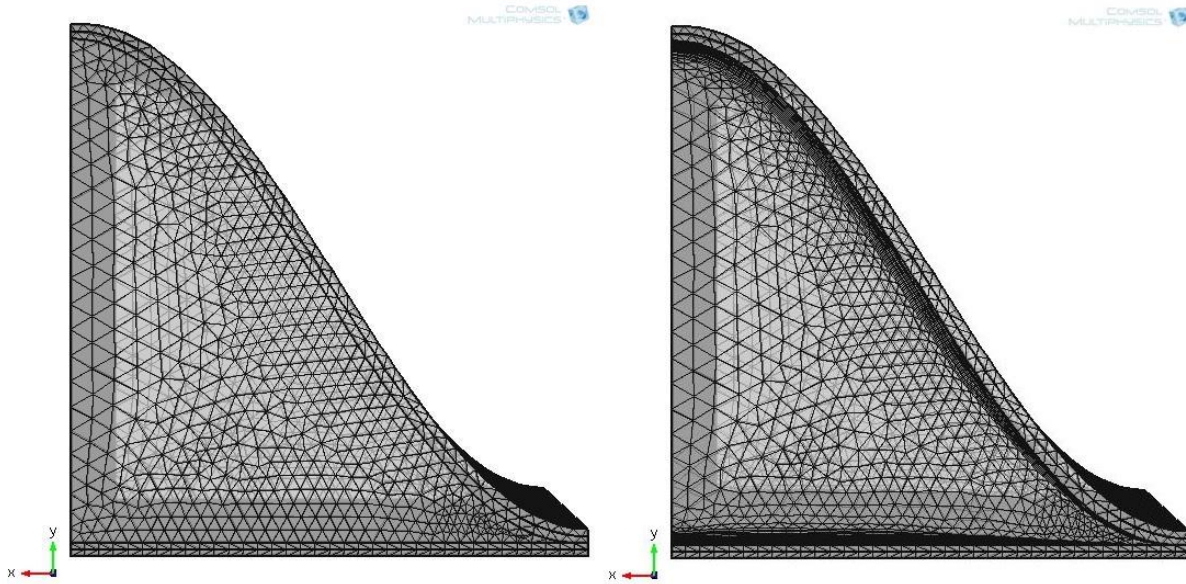


Figure 4.13 Sample cross-sectional meshes with (a) no dedicated boundary layer and (b) boundary layer (24 layers)

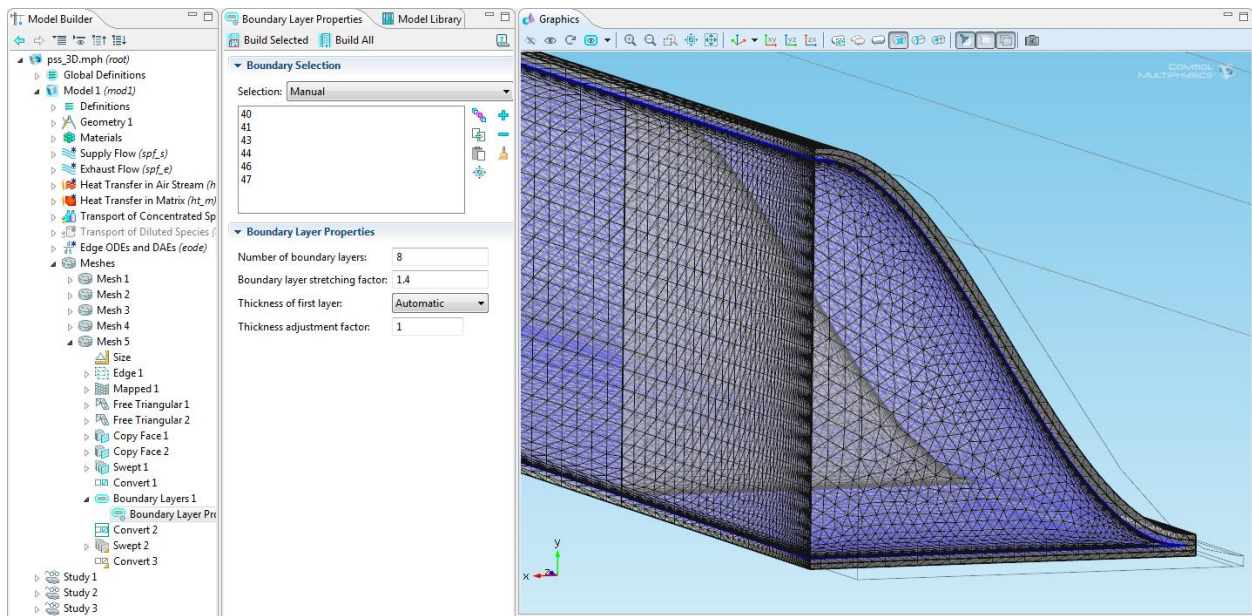


Figure 4.14 Sample mesh sequence together with associated mesh (8 layers)

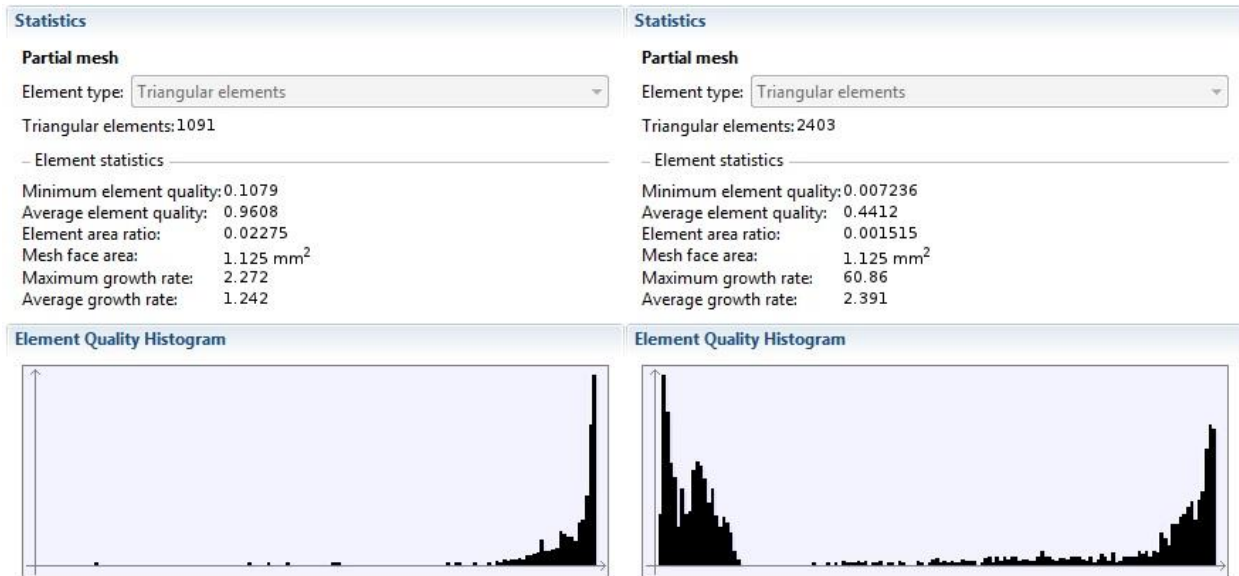


Figure 4.15 Mesh statistics of the cross-sectional mesh similar to Figure 4.13 with (a) no dedicated boundary layer and (b) boundary layer (8 layers)

While it's clear that we somehow need to address the differences between these meshes we should note that different applications (i.e. a boundary layer versus structured tetrahedral) require different mesh qualities and in comparing these two statistics directly we should keep this in mind. That said the *Minimum element quality* statistic in combination with the *Element Quality Histogram* is a telling indicator when assessing the grid quality. Beginning with the boundary of the structured tetrahedral boundary layer mesh we observe from the histogram that the element quality at any cross section is generally very high with only a few elements of lesser quality scattered away (here a value of 1 indicates an element with optimum quality). These elements are most probably artifacts of the complex geometry near the singularity and so altering the geometry around this area to a shape more amenable to the meshing process could serve to increase the minimum element quality. The same high quality elements are also present on the boundary of the dedicated boundary layer mesh only now the greater portion of the elements contained within the boundary layer causes the overall distribution to be more uniformly distributed. As we learned from the competing mesh the singularity is likely causing the most offensive elements, but now the minimum element quality is further reduced because of the additional skewed aspect ratios caused by the layer adjacent to the boundary. In general it seems like the mesh quality increases as the boundary layer grows, indicating that at least the inner layers have ratios that make them too highly distorted.

Next we observe that the number of elements is vastly increased when introducing the boundary layer mesh (here displayed using 8 layers). Contributing to this increased number is

as we notice that all the elements are triangular (or tetrahedral for domains) depending on whether we consider a boundary or a domain, respectively. The explanation for this is that while the boundary layer usually produces prism or hexagon elements depending on the surrounding mesh, the general projection operator only accepts triangular and tetrahedral elements and so if we are to use a dedicated boundary layer we have to convert this layer as well.

In conclusion then the combination of a substantially increased need for computational resources and time together with an element quality that is considered as too low, results in the dedicated boundary layer mesh being discarded in favor of the more simple mesh. On the other hand if the element quality could be improved to a certain threshold, not only on the boundary considered for simplicity here but also on the domain level where the maximum growth rate (which can be used as an indicator for jump in grid size) and element quality are still worse, then that decision should be revisited.

4.7 Pseudo-Steady State and Livelink for Matlab

The numerical model as developed so far is designed to solve the velocity problem, the conjugated heat transfer problem and the mass conservation problem for the air stream and matrix for either the supply or the exhaust part during one rotation of the wheel. Now we want to take this model one step further and solve the transient solution generated by the turning of the wheel until pseudo-steady state (or sometimes called quasi-steady state) is reached. As such the pseudo-steady solution is a transient solution that varies periodically and so even though the most important result is the pseudo-steady solution the model must be time accurate.

As discussed in Simonson and Besant (1997) the pseudo steady-state can be determined using either the periodicity of the wheel or by conservation of energy (and moisture) across the wheel. Now as we're not concerned with moisture transfer in the present state of the model we'll proceed using only the energy as an argument but it should be noted that the same line of reasoning holds for moisture. Based on an energy balance only then, pseudo-steady state is defined as the time when all the energy that is lost by one air stream is taken up by the other air stream. This means that the cyclic energy storage in the matrix over one revolution of the wheel is zero (or negligible) (Simonson and Besant, 1997). The pseudo-steady conditions for an energy balance is thus defined when,

$$\left| \frac{\dot{m}_s (H_{s,i} - H_{s,o}) - \dot{m}_e (H_{e,o} - H_{e,i})}{\dot{m}_{\min} (H_{s,i} - H_{e,i})} \right| \leq \textit{tolerance} \quad (4.25)$$

where the enthalpy terms are the velocity weighted bulk enthalpy defined as

$$H_b = \frac{1}{A_c w_b} \int_{A_c} w H dA_c \quad (4.26)$$

and the tolerance determines how stringent the solution is defined.

To ensure that eq. (4.25) gives the pseudo-steady solution Simonson and Besant (1997) suggests that periodicity of the wheel is checked by calculating the effectiveness after each revolution of the wheel. Periodicity is reached when the change in effectiveness is zero (or negligible),

$$\left| \frac{\partial \varepsilon}{\partial t} \right| = \frac{|\varepsilon - \varepsilon^0|}{p_s + p_e} \leq \textit{tolerance} \quad (4.27)$$

where ε is the total energy (enthalpy) effectiveness defined as the average of the supply and exhaust side effectivenesses (ε^0 is the effectiveness of the previous rotation of the wheel),

$$\varepsilon = \frac{\dot{m}_s (H_{s,i} - H_{s,o}) + \dot{m}_e (H_{e,o} - H_{e,i})}{2\dot{m}_{\min} (H_{s,i} - H_{e,i})} \quad (4.28)$$

The sensible heat transfer effectiveness, assuming constant specific heat, is given as,

$$\varepsilon = \frac{\dot{m}_s (T_{s,i} - T_{s,o}) + \dot{m}_e (T_{e,o} - T_{e,i})}{2\dot{m}_{\min} (T_{s,i} - T_{e,i})} \quad (4.29)$$

As the above equations (4.25,4.27-4.29) involves using properties from both the supply and exhaust section of the wheel it is clear that we need to have access to two sets of solutions – one for the supply part and one for the exhaust part – to evaluate if pseudo-steady state has been reached. In other words we need to progress the solution forward in time meaning that the numerical model as defined in this chapter needs to alternate between solving for the supply and exhaust section of the wheel. Then at the end of each rotation we need to evaluate whether or not pseudo-steady state has been achieved, that is if the transient solutions has converged.

At the level of the numerical model this entails using the previous solution at time $t = t_f$ where $t_f = t_0 + \textit{period}$ (t_0 is the start of the period) for one section as the initial values for the simulation of the next section. That way we impose a continuous temperature for the matrix (and for the properties of the air stream). To simulate the actual turning of the wheel (assuming that the supply and exhaust air stream are arranged in a cross-flow arrangement) we need to reconfigure the boundaries on which the inlet and outlet conditions are defined to reflect the reversal of the flow direction. At this point it is prudent to remind ourselves that the flow

geometry solution is stationary indicating that some level of error has been introduced by assuming that the velocity profile develops instantaneously at the moment of transition. Alas the effect is likely to be small as long as the mass flow rate is sustained at the current level, but could become a concern when the mass flow rate is reduced.

Now to combine the need to progress to solution forward and evaluate if the solutions has converged with the changes made at the level of the numerical model it is clear that we need some high level language that allows us to develop algorithms and evaluate data in a way that the modeling platform in the *COMSOL Desktop* is not designed for. The solution is to use the *Livelink for MATLAB* interface which allows us to combine and use *COMSOL Multiphysics* together with *MATLAB* by creating a bidirectional integration between these modeling environments. This interface includes the *COMSOL API* so that for each operation done in the *COMSOL Desktop* there is a corresponding command that is entered at the *MATLAB* prompt. Thus it allows the user to save the numerical model with the geometry, variables, couplings, physics, and so forth as constructed in the *COMSOL Desktop* as a M-file for further processing.

This enables us to use the open-ended technical computing environment of *MATLAB* for programmatic control for setting up and running the numerical model using repetitive operations like the *while* loop (or alternatively the *for* loop) and controls like *if-else*. Now if we combine that together with communication between *COMSOL Multiphysics* and *MATLAB* variables and the option to call individual study nodes as defined in the numerical model in the *MATLAB* workspace, it is easy to envisage how the complete pseudo-steady state numerical model might be constructed. The actual process is not easily communicated as the language and functions used in *MATLAB* are specific to the *Livelink for MATLAB* interface and is best learned by trial and error. The resulting algorithm for progressing the solution together with the changes done at the level of the numerical model (which is of course implemented at the level of the *Livelink for MATLAB* specific language used in *MATLAB* rather than manually in the *COMSOL Desktop*) is given in Appendix B.

The complete model for obtaining the pseudo-steady state solution and describing the transient nature of the wheel operation is thus a product of the numerical model as constructed using the modeling platform of *COMSOL Multiphysics* and the algorithm developed in *MATLAB* using the *Livelink for MATLAB* interface.

CHAPTER 5

RESULTS AND DISCUSSION

The numerical simulations were carried out using a fully coupled and direct solver for all the study nodes – the most robust scheme – as the mesh is constructed in such a highly controlled manner that it does not lend itself to the multigrid methods of the iterative solver (it generates errors as the mesh cannot be appropriately partitioned without generating inverted elements) and as the problem is posed in such a way that the segregated solver cannot be initiated. Using the numerical algorithm as defined in Appendix B the solution for the supply and exhaust sections was progressed until the convergence criteria of equations (4.25) and (4.27) were reached.

Calculations were conducted on the Kongull Linux Cluster (CentOS 5.3 Linux cluster running Rocks) using 1 x Dell Intel Xeon based compute nodes, each with 2 x Intel(R) Xeon(R) CPU E5-2670 @ 2.60GHz 8-core (Sandy Bridge) processors and 32GB DDR3 1600 MHz memory. To set up the job sent to the cluster for processing *COMSOL Commands on Linux* (see the *COMSOL Multiphysics Reference Manual*) were used together with Kongull (i.e. CentOS 5.3 Linux Cluster) specific commands. The resulting job script is given in Appendix C using the Message Passage Interface (MPI) system.

As a consequence of not succeeding to complete the numerical model in a timely fashion only a few simulations to convergence has been performed, and as such no extensive library of different data sets has been compiled. Neither has the tolerance criteria for the energy balance nor the periodicity been subject to analysis and so it has not been checked if making them more or less stringent will change the predicted effectiveness.

5.1 Mesh Refinement Study

The lack of different data sets makes it impossible to track any characteristic output parameter and as such no mesh refinement study has been conducted to find the best mesh size and fineness. The complete mesh used in this thesis is therefore based on a qualitative judgment only and represents a balance between maintaining the minimum element quality and the cross-sectional and swept meshes at an acceptable level while trying to keep the total number of elements at a minimum. The mesh statistics is given below in Figure 5.1 along with the associated mesh. For the physics currently employed in the simulations combined with this mesh (which is thought to be intermediate with respect to number of elements) the number of degrees of freedom was 603472 (plus 226087 internal DOFs) and the computational time

needed to simulate one rotation of the wheel was approximately 6-8 hours depending on the number of computational nodes used.

If such a study were to be conducted however *COMSOL Multiphysics* allows us to track any variable or mathematical expression of variables at a single point of interest or use some operation (integral, average, minimum, maximum, etc.) performed over one or more of the domains, boundaries or edges. In our case the best option might be to track the bulk temperature at the outflows for both the supply and exhaust air streams which are already defined and solved for using the nested general projection combined with the Edge ODE and DAEs interface and general extrusion operator.

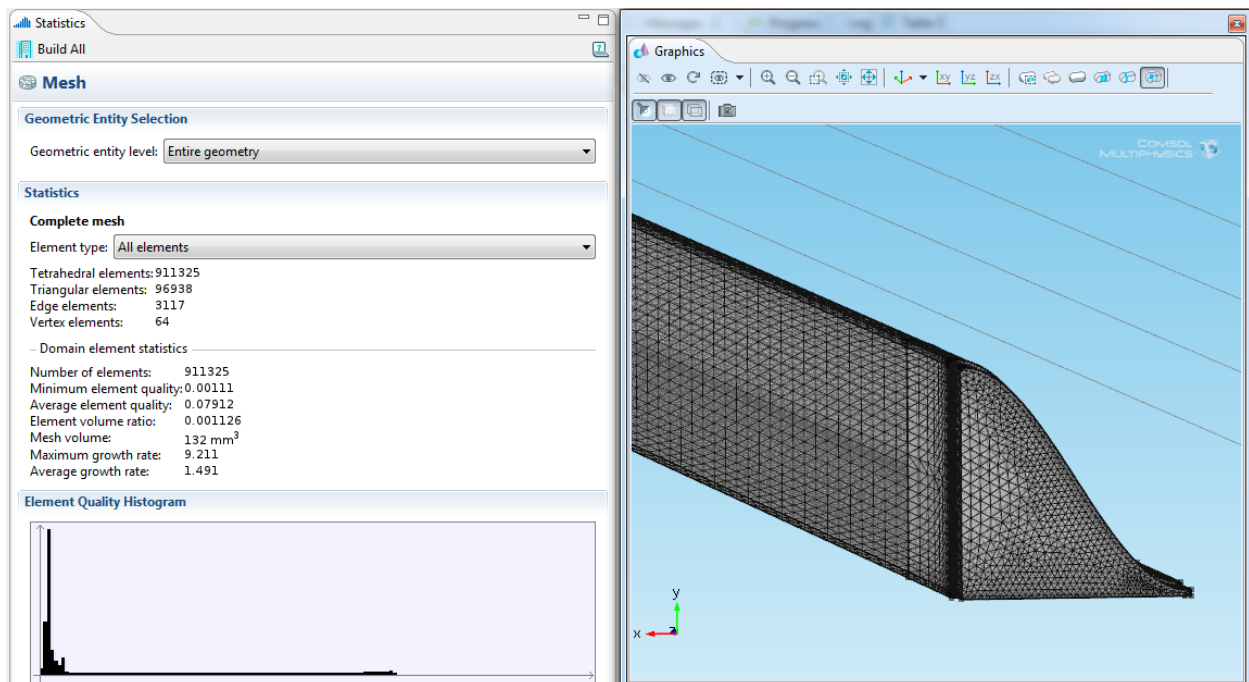


Figure 5.1 Mesh statistics and the associated mesh used in the simulations

Next we would typically have to define some parameter or parameters in our case as we would probably want to check both the cross-sectional mesh and the swept mesh, and then use those in the relevant *size features* and *number of elements* properties of the cross-sectional and swept mesh, respectively. Then using a parametric sweep with our dummy variable defined above we should sweep through a wide range of maximum mesh sizes to capture the convergence effect. Now while we should arguably solve for the pseudo-steady state solution this would take excessively long time and instead it may be prudent to just solve for one rotation of the wheel or even only one of the sections.

After computing the simulations we should join the relevant data sets that compares the tracking parameter at each mesh size with the value of the tracking parameter that is considered to be a reliable solution (which would typically be the finest mesh size). As we want to capture the convergence effect the data sets should be subtracted from each other and the result (here the difference between the bulk temperatures at the outflows) plotted against the tracking parameter.

5.2 Validation of Formulation

As there was only a handful of simulations performed with the complete model, and as the computational times required are extensive, the process was controlled by using an *for*-loop with only two full rotations of the wheel simulated instead of going for full convergence. As such the values presented in the following sections will not represent converged values and is only for demonstration, but the initial condition for the matrix temperature was continually updated with the previously conducted simulations and so it is expected that the transient solutions will convergence with a small number of consecutive turns of the wheel. Moreover the ripples was not adequately smoothed out in the simulations, and so we might envisage to extend the flow field further or improve the mesh (i.e. more dense at the ends) to improve performance. It may be that the ripples will be smoothed out with more consecutive turns of the wheel as well.

In validating the formulation we will use the predicted sensible heat transfer effectiveness of equation (4.29) rather than the total energy (enthalpy) effectiveness of equation (4.28) as no moisture is transferred is in the present analysis (even if there is condensation) and because the effectiveness relations given in the literature is for sensible heat transfer only. Using the modeling parameters of Table 4.1 and the modified sine duct Nusselt number of Figure 4.6 the sensible heat transfer effectiveness becomes:

$$\varepsilon = \frac{\dot{m}_s (T_{s,i} - T_{s,o}) + \dot{m}_e (T_{e,o} - T_{e,i})}{2\dot{m}_{\min} (T_{s,i} - T_{e,i})} = 0.776 \quad (4.30)$$

where $T_{s,o}$ and $T_{e,o}$ are the time-averaged temperatures at the respective outflows over the time interval $\frac{1}{3}p \leq t \leq p$ (see Figures 5.3 and 5.4 of the test case).

As the temperature has not been time-averaged over the interval $0 \leq t \leq (1/3)p$ the final effectiveness should be somewhat higher (while the convergence will most probably pull in the other direction) but the interval has been neglected because of some disturbance, presumably from the ripples and the fact that the transient solutions has not converged.

To find how this effectiveness compare to that of the literature we have to define the overall number of heat transfer units (NTU_0) and overall matrix heat capacity (Cr^*_0) from the modeling parameters. In the case of equal flow areas, heat transfer coefficients and mass flow rates on the hot and cold side, NTU_0 and Cr^*_0 simply becomes (Tunaa, 2013),

$$NTU_0 = \frac{hA_s}{2(\dot{m}C_p)} \quad (4.31)$$

where h is the fully developed averaged peripheral convective heat transfer coefficient, A_s is the heat transfer surface are, \dot{m} is the mass flow rate and C_p is the specific heat capacity at constant pressure of the air stream.

$$Cr^*_0 = \frac{(MC_p)_m N}{(\dot{m}C_p)} \quad (4.32)$$

where M is the mass of the wheel, $C_{p,m}$ is the specific heat capacity at constant pressure of the matrix, and N is the angular speed of the wheel.

In order to find NTU_0 we begin by calculating the heat transfer surface area as

$$\begin{aligned} A_s &= \frac{1}{2} \times \text{rotor cross-sectional area} \times \text{rotor length} \times \text{matrix packing density } \beta \\ &= \frac{1}{2} \times \frac{\pi}{4} (0.9)^2 \text{ m}^2 \times 0.1 \text{ m} \times 3041 \frac{\text{m}^2}{\text{m}^3} = 96.75 \text{ m}^2 \end{aligned} \quad (4.33)$$

where the matrix packing density is given as $\beta = 4\sigma/D_h$ and the total heat transfer surface area is $A = 2A_s$ as the wheel is divided into equal sector angles.

The fully developed convective heat transfer coefficient can be found as,

$$h = Nu \cdot \frac{k}{D_h} = 52.5 \frac{W}{\text{m}^2 K} \quad (4.34)$$

where the mixture thermal conductivity has been evaluated at the mean temperature

$$T = (1/2) \cdot (T_{s,i} + T_{e,i}).$$

From the foregoing values together with the mass flow rate and the specific heat capacity at constant pressure, again evaluated at the mean temperature, we get,

$$NTU_o = \frac{hA_s}{2(\dot{m}C_p)} = 5.03 \quad (4.35)$$

To determine Cr_o^* , we first determine the matrix mass as,

$$\begin{aligned} M &= \text{rotor cross-sectional area} \times \text{rotor length} \times \text{matrix material density} \\ &\quad \times \text{matrix solidity} \\ &= \frac{\pi}{4} (0.9^2) \text{m}^2 \times 0.1 \text{m} \times 2700 \text{kg/m}^3 \times (1 - 0.925) = 12.9 \text{kg} \end{aligned} \quad (4.36)$$

Knowing the matrix mass, its heat capacity rate is computed as,

$$Cr = (MC_p)_m N = 12.9 \text{kg} \times 900 \text{J/kg} \cdot \text{K} \times \frac{20}{60} \text{rev/s} = 3879 \text{W/K} \quad (4.37)$$

Knowing Cr and the mass flow rate and the specific heat capacity at constant pressure for the air stream, we have,

$$Cr_o^* = \frac{(MC_p)_m N}{(\dot{m}C_p)} = 7.69 \quad (4.38)$$

To include the effect longitudinal heat conduction in the matrix we need another dimensionless group,

$$\lambda = \frac{k_w A_{fr} (1 - \sigma)}{LC_{\min}} = 0.15 \quad (4.39)$$

An empirical effectiveness correlation expressed in terms of NTU_o and Cr_o^* for a sensible regenerative heat exchanger, valid for $\varepsilon \leq 0.9$ and $C^* = C_{\min}/C_{\max} = 1$, is given as (Shah et al. , 2003),

$$\varepsilon = \frac{NTU_o}{1 + NTU_o} \left[1 - \frac{1}{9(Cr_o^*)^{1.93}} \right] \left(1 - \frac{C_\lambda}{2 - C^*} \right) = 0.767 \quad (4.40)$$

where

$$C_\lambda = \frac{1}{1 + NTU_o(1 + \lambda\Phi)/(1 + \lambda NTU_o)} - \frac{1}{1 + NTU_o}, \Phi = \left(\frac{\lambda NTU_o}{1 + \lambda NTU_o} \right)^{1/2} \quad (4.41)$$

Thus we have an expected value for a heat wheel with the same characteristics as the one employed in the present analysis that are somewhat less than the predicted effectiveness

of the current scheme which is to be expected because of the additional heat transfer in the entrance region (not accounted for in the analysis above). Even if we narrow in on the details though by not assuming equal heat transfer coefficients and specific heats (which are very good approximations) the predicted effectiveness should differ only marginally. These discrepancies should clearly be explored further in respect to both the numerical model and the hand calculations, but again because of time concerns (also with long simulation times) this has not been done in this thesis. Of special concern should be to mitigate the ripples as discussed in the velocity problem of the numerical model (section 4.3). Using the methodology above the effectiveness should also be checked for a host of different values of NTU_0 and Cr_0^* corresponding to a set of different modeling parameters to ensure consistency. In addition to this validation it may be prudent to check the temperature profiles obtained with the current formulation against some experimental data but lacking both data for the simulations and any reliable experimental data this has not been done.

5.3 Test Case

To illustrate the proposed formulation, simulation results of a test-case, compromising heat transfer in a selected heat wheel, are presented. The input data used in the simulations can be found in Table 4.1. To reiterate the inlet air temperatures and relative humidities are $T_{supply} = -10^\circ C$ and $T_{exhaust} = 20^\circ C$, and $\phi_{supply} = 0.20$ and $\phi_{exhaust} = 0.40$, respectively, whereas the mass flow rates are balanced and equal to $\dot{m}_{supply} = \dot{m}_{exhaust} = 0.5 \text{ kg} / \text{s}$.

In order to obtain insight on the pseudo-transient nature of the wheel, the evolution of the temperature distribution in the matrix is examined over one rotation of the wheel (Figure 5.2). In addition the bulk cold and dry supply air and the bulk hot and humid exhaust air temperature distributions are given in Figure 5.3 and 5.4, respectively. As can be seen, the matrix absorbs heat during the exhaust section of the wheel and releases this heat in the supply section of the wheel. All of these temperatures profiles is very reminiscent of and shows good agreement with the distributions as presented in Holmberg (1977) for a wheel with balanced flows and $NTU_0 = 5$ and $Cr_0^* = 5$, respectively.

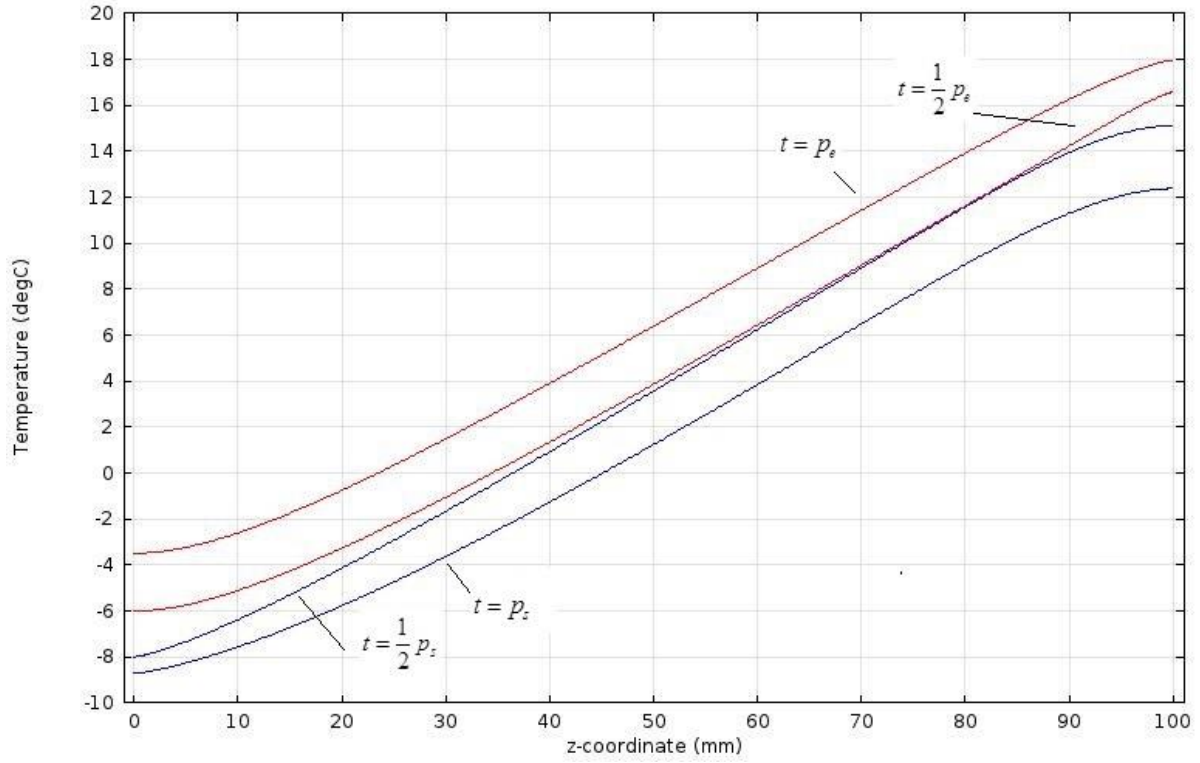


Figure 5.2 Matrix temperature distribution over one rotation of the wheel

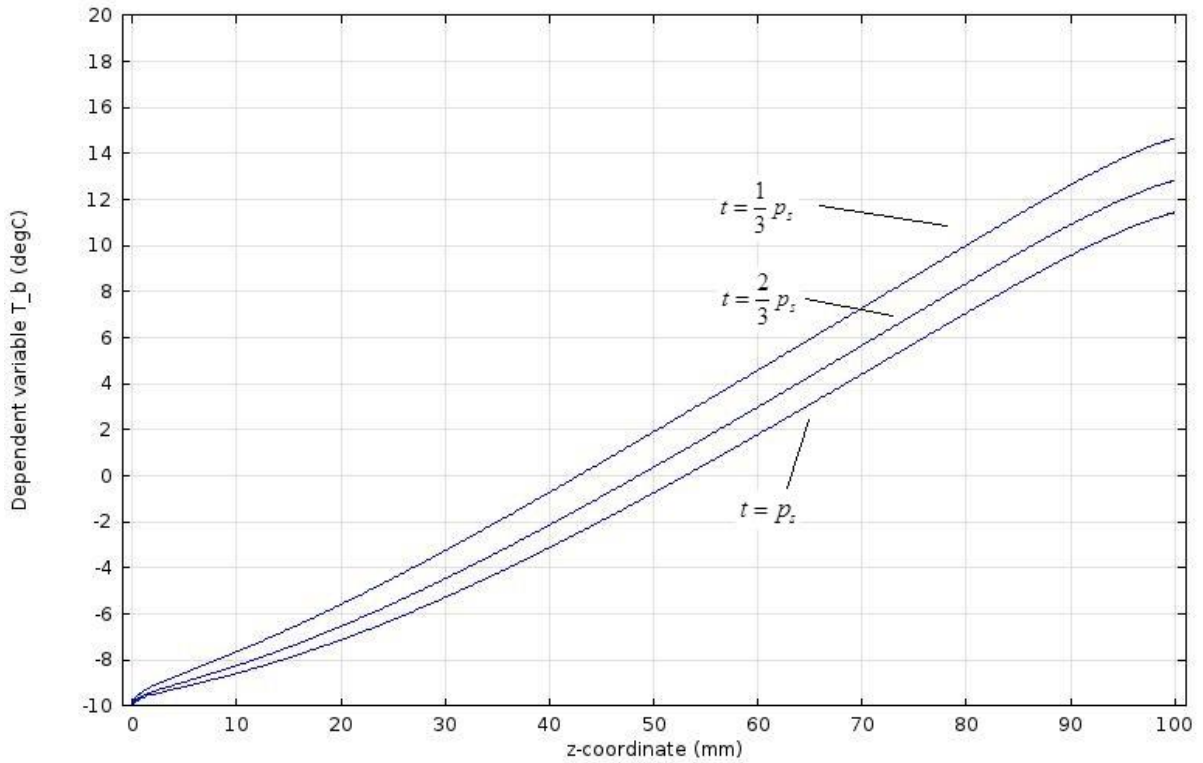


Figure 5.3 Bulk temperature distribution over the supply section of the wheel

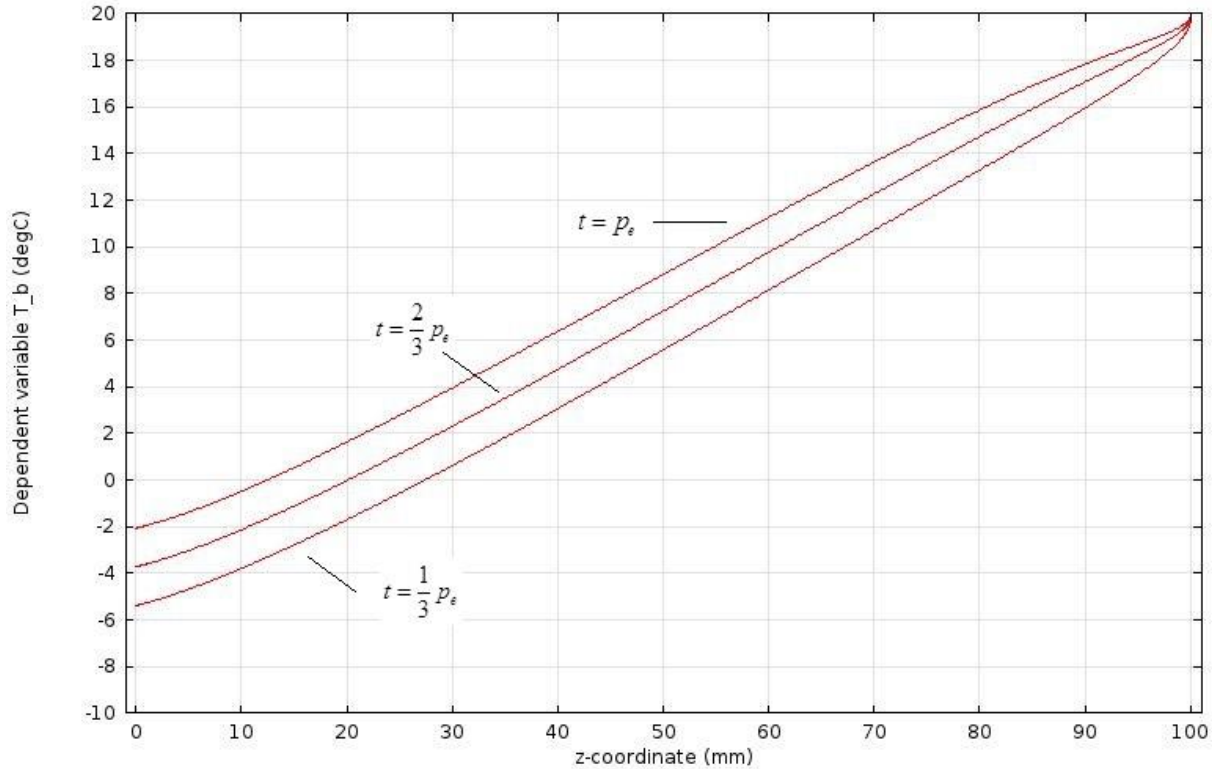


Figure 5.4 Bulk temperature distribution over the exhaust section of the wheel

The three-dimensional flow geometry in the entrance region and for the fully developed flow was given in Figures 4.3 and 4.4, respectively, and need not be repeated here. The effect of this flow geometry and the local peripheral heat flux distribution on the resulting cross-sectional temperature profile is illustrated in Figure 5.5 for the exhaust section of the wheel at $z = 40\text{ mm}$ (i.e. a flow length of 60 mm) and time $t = t_f$ (3.0s).

As displayed, there is a considerable temperature difference between that of the wall and the near-stagnant pockets in the regions of low wall-to-wall distance, and that of the centroid with fast flowing air. As such these pockets of near-stagnant air represents cold spots and will along with the air immediately adjacent to the wall around the periphery be subject to condensation even if the bulk humidity gives no indication that condensate will begin to precipitate out of the air. This becomes clear when considering a relative humidity profile for the exhaust section of the wheel at the same cross-section and time (Figure 5.6), and a plot of the relative humidity at the wall together with the bulk relative humidity of the associated cross-sections versus the flow length (Figure 5.7).

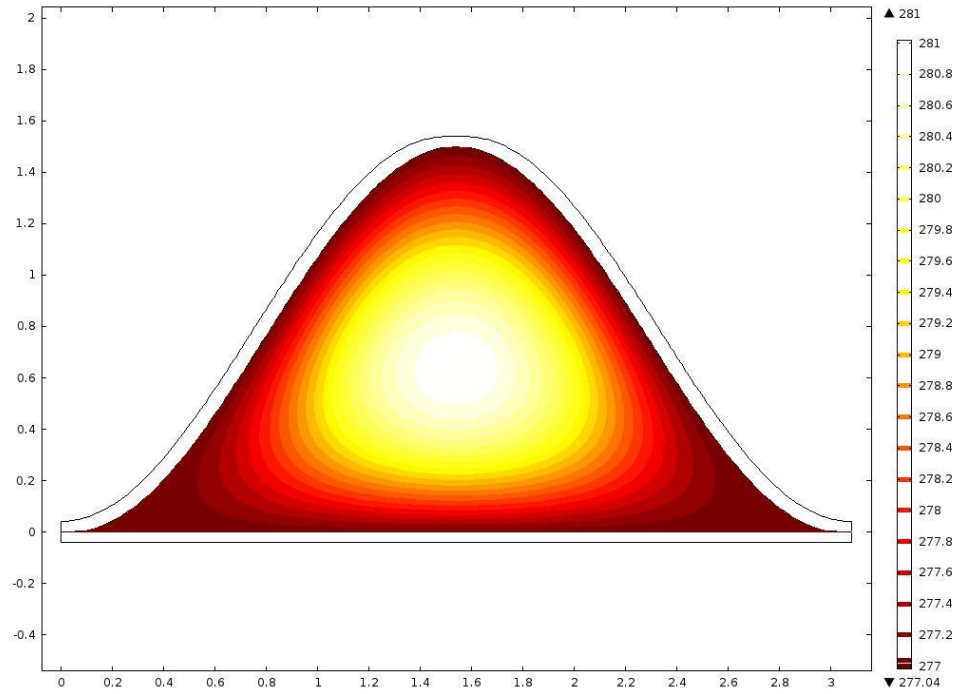


Figure 5.5 Contour plot of the air stream temperature profile at $z = 40$ mm

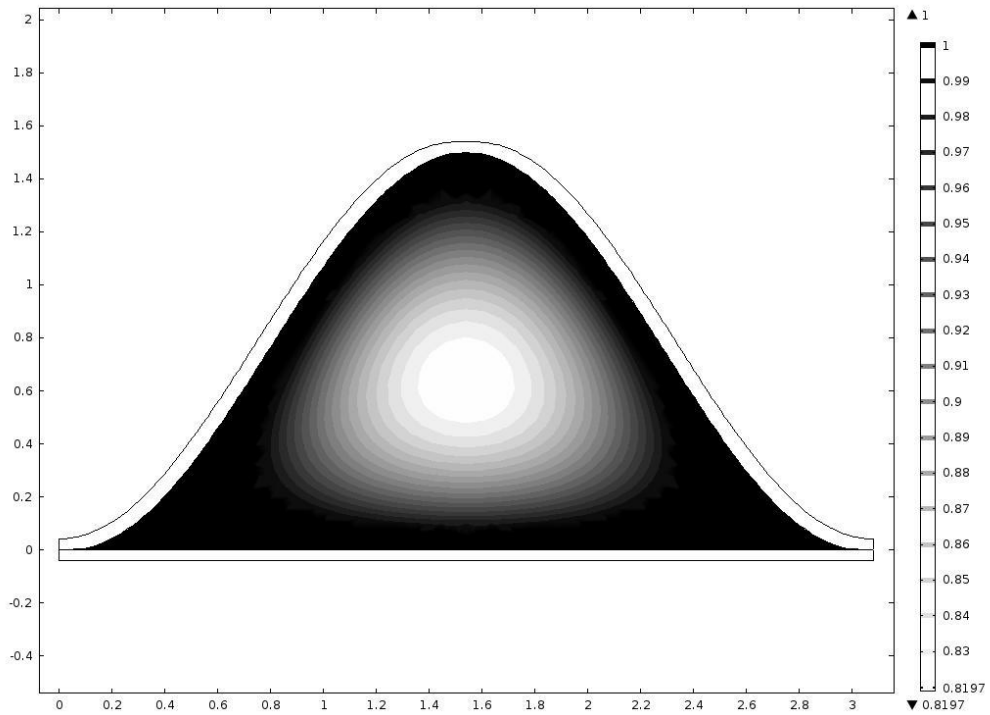


Figure 5.5 Contour plot of the relative humidity profile at $z = 40$ mm with black regions indicating condensation/frost.

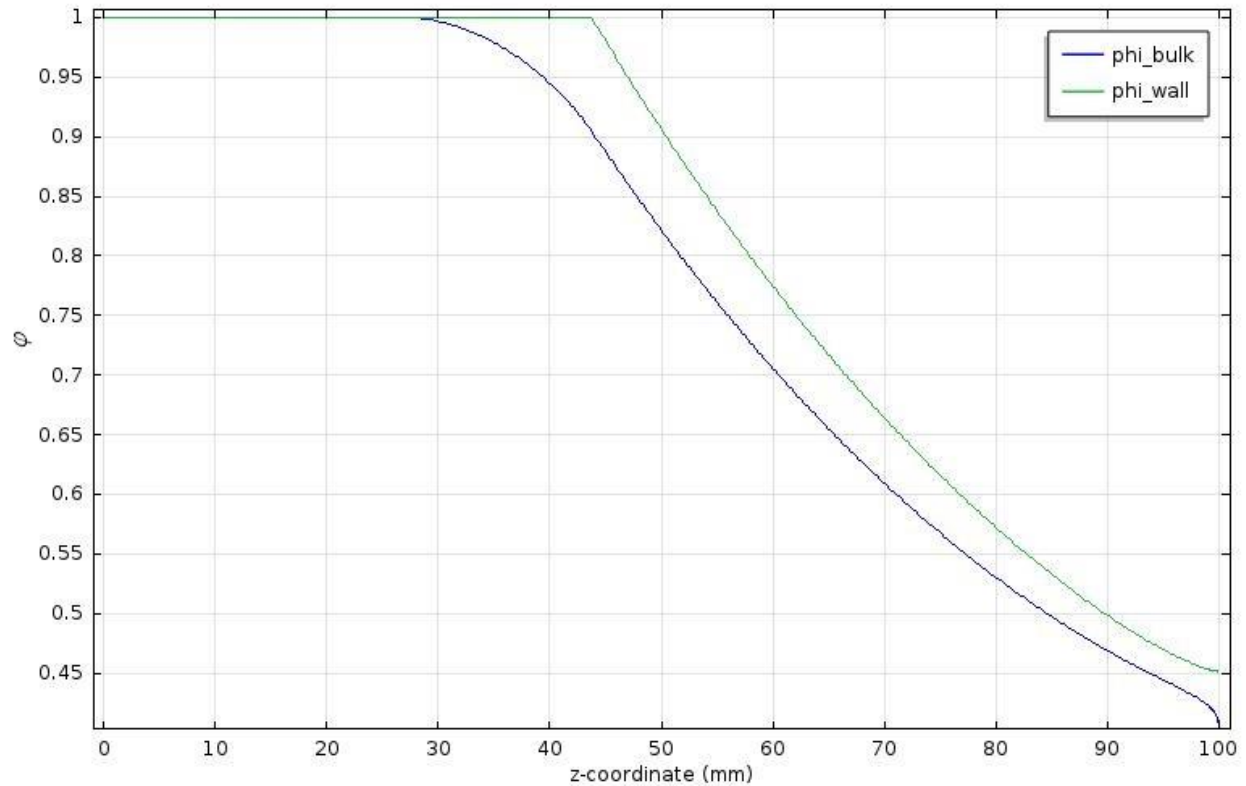


Figure 5.7 Local wall relative humidity versus bulk humidity for the exhaust section of the wheel.

These figures demonstrate that condensation/frosting conditions will exist locally within the wheel and moreover that the limits clearly will be influenced by the geometry of the wheel. As seen the moisture in the air will begin to precipitate out of the air in the pockets already at $z = 43\text{ mm}$, continually increasing as the temperature drops further to envelop the whole cross-section at $z = 28\text{ mm}$, where the bulk relative humidity finally reaches unity. This discrepancy might be a cause for concern as the condensation/frosting limits established in e.g. Holmberg (1989) and Simonson et al. (1997) is based on whether the supply air (as in bulk relative humidity) is able to pick up all of the condensate precipitated out of the exhaust air or if a zone of frost/condensation will be left behind. Obviously even if the supply bulk relative humidity drops below unity, indicating that all the condensate has been picked up, there may still be reservoirs of frost/condensate left in the near-stagnant pockets of condensate also transferred to the supply section.

CHAPTER 6

CONCLUSIONS AND AREAS OF FUTURE STUDY

A three-dimensional and transient mathematical model for the heat transfer in regenerative heat exchangers has in this thesis been developed from physical principles, with efforts aimed at a detailed description of the thermally and hydraulically developing flow problem. The mathematical model was implemented using the computational package *COMSOL Multiphysics with Livelink for MATLAB* rather than an imperative programming language like *Fortran*. As such the resulting model represents a step towards analyzing the multiphysics phenomena of heat and mass transfer occurring in regenerative heat exchangers in full three-dimensional detail by utilizing automated state-of-the-art numerical analysis methods and powerful visualizations tools instead of settling with one-dimensional models carrying less information. The current procedure makes for a more user-friendly approach by allowing for ongoing visual feedback, making the entire process more streamlined, less prone to error and the results easier to analyze.

The model developed in this thesis is unique in that proper scaling analysis has been performed to complete the simultaneously developing Nusselt numbers in the entrance region from incomplete tabular data sources, and in that a local peripheral Nusselt number function has been developed from the flow geometry to reflect the varying peripheral local heat flux around the periphery. In addition it also considers an extended flow field designed to improve the flow field, to negate ripple effects resulting from unphysical temperature gradients, and to ensure that the heat fluxes and temperature fields at the inlets are continuous.

Results from the simulation of a test case considered in this thesis show that the local properties may deviate significantly from the bulk properties, suggesting that condensation may be present locally in pockets of near-stagnant regions for a considerable length of the wheel. The condensate precipitated out in these regions will not be captured by one-dimensional formulations considering only bulk flow and so they run the risk of greatly underestimating the amount of condensate actually forming.

The numerical model presented has not been validated extensively and there is a need for further validation to ensure that the model provides consistent results. In addition the ripples should be revisited to see if they can be further mitigated. The model has neither been subject to a mesh refinement study nor has the modeling parameters been analyzed for sensitivity. As such there is a clear need for further research regarding these issues and in particular the influence of the characteristic parameters such as the mass flow rate and the angular velocity of the wheel on the performance.

Regardless of the necessity for further investigation the proposed three-dimensional numerical model should provide an excellent platform for future studies that aims to incorporate sorption mass transfer and/or condensation and frost. At present there does not seem to be adequate built-in physics to support all of the additional considerations needed for analyzing the local diffusional effects or sorption isotherm in the desiccant, nor the mass transfer associated with change of phase resulting from condensation or frost. As additional modules is continually added to the *COMSOL Multiphysics* platform this may change in the future. There are however *PDE Interfaces* and *ODE and DAE Interfaces* available that might be used to manually define the physics needed under the *Mathematics Module* along with options to control the mesh (*Moving Mesh*) to take into account the changing interface caused by condensate precipitating out of the air stream.

REFERENCES

- Bejan, A. (2004). *Convection Heat Transfer*: Wiley.
- Bilodeau, S., Brousseau, P., Lacroix, M., & Mercadier, Y. (1999). Frost formation in rotary heat and moisture exchangers. *International Journal of Heat and Mass Transfer*, 42(14), 2605-2619. doi: [http://dx.doi.org/10.1016/S0017-9310\(98\)00323-8](http://dx.doi.org/10.1016/S0017-9310(98)00323-8)
- Fischer Jr, J. C. (1988). High efficiency sensible and latent heat exchange media with selected transfer for a total energy recovery wheel: Google Patents.
- Hirsch, C. (2007). *Numerical Computation of Internal and External Flows: The Fundamentals of Computational Fluid Dynamics: The Fundamentals of Computational Fluid Dynamics* (Vol. 1): Butterworth-Heinemann.
- Holmberg, R. B. (1977). Heat and mass transfer in rotary heat exchangers with nonhygroscopic rotor materials. *Journal of Heat Transfer*, 99(2), 196-202.
- Holmberg, R. B. (1989). Prediction of condensation and frosting limits in rotary wheels for heat recovery in buildings. *ASHRAE transactions*, 95, 64-69.
- Jeong, J.-W., & Mumma, S. A. (2005). Practical thermal performance correlations for molecular sieve and silica gel loaded enthalpy wheels. *Applied Thermal Engineering*, 25(5-6), 719-740. doi: <http://dx.doi.org/10.1016/j.applthermaleng.2004.07.018>
- Ray, S., & Misra, D. (2010). Laminar fully developed flow through square and equilateral triangular ducts with rounded corners subjected to H1 and H2 boundary conditions. *International Journal of Thermal Sciences*, 49(9), 1763-1775. doi: <http://dx.doi.org/10.1016/j.ijthermalsci.2010.03.012>
- Shah, R. K. (1975). Laminar flow friction and forced convection heat transfer in ducts of arbitrary geometry. *International Journal of Heat and Mass Transfer*, 18(7-8), 849-862. doi: [http://dx.doi.org/10.1016/0017-9310\(75\)90176-3](http://dx.doi.org/10.1016/0017-9310(75)90176-3)
- Shah, R. K., & London, A. L. (1978). *Laminar flow forced convection in ducts: a source book for compact heat exchanger analytical data* (Vol. 1): Academic press.
- Shah, R. K., Sekuli, & P., D. Fundamentals of Heat Exchanger Design: John Wiley & Sons.
- Sherony, D., & Solbrig, C. (1970). Analytical investigation of heat or mass transfer and friction factors in a corrugated duct heat or mass exchanger. *International Journal of Heat and Mass Transfer*, 13(1), 145-159.
- Simonson, C. (2007). Heat and energy wheels. *Encyclopedia of Energy Engineering and Technology*, 2, 794-800.
- Simonson, C., Besant, R., & Wilson, G. (1997). Condensation and frosting in energy wheels. *ASME-PUBLICATIONS-HTD*, 339, 161-170.
- Simonson, C. J. (1998). Heat and moisture transfer in energy wheels.
- Simonson, C. J., & Besant, R. W. (1997). Heat and Moisture Transfer in Desiccant Coated Rotary Energy Exchangers: Part I. Numerical Model. *HVAC&R Research*, 3(4), 325-350. doi: 10.1080/10789669.1997.10391381
- Sphaier, L. A., & Worek, W. M. (2004). Analysis of heat and mass transfer in porous sorbents used in rotary regenerators. *International Journal of Heat and Mass Transfer*, 47(14-16), 3415-3430. doi: <http://dx.doi.org/10.1016/j.ijheatmasstransfer.2004.01.016>
- Tunaa, E. (2013). Rotary Heat Exchanger - Literature Study on Sorption Processes, Condensation and Frosting. 49.